North American continental margin records of the Paleocene-Eocene thermal maximum: Implications for global carbon and hydrological cycling

Cédric M. John,[1,2] Steven M. Bohaty,[1,3] James C. Zachos,[1] Appy Sluijs,[4] Samantha Gibbs,[3,5] Henk Brinkhuis,[4] and Timothy J. Bralower[5]

[1]   The impacts of the Paleocene-Eocene thermal maximum (PETM) ($\sim$55 Ma), one of the most rapid and extreme warming events in Earth history, are well characterized in open marine and terrestrial environments but are less so on continental margins, a major carbon sink. Here, we present stable isotope, carbonate content, organic matter content, and C:N ratio records through the PETM from new outcrop sections in California and from cores previously drilled on the New Jersey margin. Foraminifer $\delta^{18}O$ data suggest that midlatitude shelves warmed by a similar magnitude as the open ocean ($5°C–8°C$), while the carbon isotope excursion (CIE), recorded both in carbonate and organic matter $\delta^{13}C$ records, is slightly larger ($3.3–4.5‰$) than documented in open ocean records. Sediment accumulation rates increase dramatically during the CIE in marked contrast to the open ocean sites. In parallel, mass accumulation rates of both organic and inorganic carbon also increased by an order of magnitude. The estimated total mass of accumulated carbon in excess of pre-CIE rates suggests that continental margins, at least along North America, became carbon sinks during the CIE, mainly because of weathering feedbacks and rising sea level. This result is significant because it implies that the negative feedback role of carbon burial on continental margins was greater than previously recognized.

1.   Introduction

[2]   The Paleocene-Eocene thermal maximum (PETM) was an interval of rapid, transient (170–220 ka) global warming characterized by a prominent negative carbon isotope excursion (CIE) and massive dissolution of seafloor carbonates [*Kennett and Stott*, 1991; *Koch et al.*, 1992; *Zachos et al.*, 2003, 2005; *Sluijs et al.*, 2006]. The onset of the CIE marks the base of the Eocene, and is interpreted as representing the rapid injection of a large mass (>2000 Gt C) of ^{13}C-depleted carbon to the atmosphere and ocean [*Dickens et al.*, 1997; *Zachos et al.*, 2005]. Though the exact source of ^{13}C-depleted carbon has yet to be determined, several potential candidates have been proposed, including dissociation of methane hydrates [*Dickens et al.*, 1995] and thermal combustion or oxidation of sedimentary organic matter [*Svensen et al.*, 2004] or a combination of sources [*Sluijs et al.*, 2007].

[3]   Regardless of source, the excess carbon was eventually removed from the ocean/atmosphere via biogeochemical feedbacks, primarily intensified silicate weathering and subsequent increased carbonate deposition [*Dickens et al.*, 1997; *Bains et al.*, 2000; *Ravizza et al.*, 2001]. Evidence for intensified chemical weathering as a consequence of a more energetic hydrological cycle during the PETM is recorded widely at middle and high latitudes in both hemispheres [*Pagani et al.*, 2006b]. The weathering signal is most acute during the phase of progressive return to higher $\delta^{13}C$ values (the "recovery") which is marked by a shift in clay mineralogy in many shelf sections [*Bolle et al.*, 1998a, 2000b, 2000c; *Gibson et al.*, 2000], carbonate-rich sediments in the deep sea [*Robert and Kennett*, 1994; *Kelly et al.*, 2005; *Zachos et al.*, 2005], and intensive pedogenesis on land [*Clechenko et al.*, 2007]. The change in weathering style was highly regional, with subtropical regions showing evidence of increased seasonality or even transient drying during the initial phase of the PETM. This is well documented in Pyreneans sections where higher rates of land erosion and massive fan deposits highlight a more efficient physical weathering of the bedrock [*Schmitz and Pujalte*, 2003, 2007], and in paleosols of the Bighorn Basin which record evidence of transient drying and alternate wet/dry cycles [*Wing et al.*, 2005; *Kraus and Riggins*, 2007].

[1]Department of Earth and Planetary Sciences, University of California, Santa Cruz, California, USA.

[2]Now at Department of Earth Science and Engineering, Imperial College London, London, UK.

[3]Now at School of Ocean and Earth Sciences, National Oceanography Centre, Southampton, UK.

[4]Palaeoecology, Institute of Environmental Biology, Utrecht University, Utrecht, Netherlands.

[5]Department of Geosciences, Pennsylvania State University, University Park, Pennsylvania, USA.
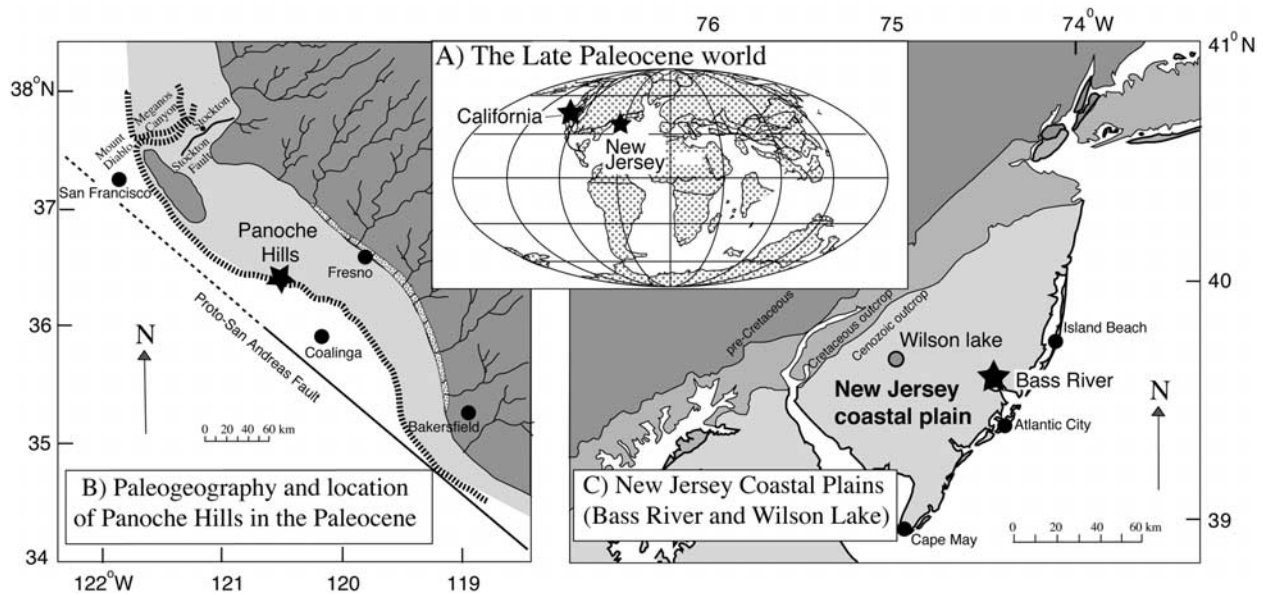
Figure 1. Location and paleogeography. (a) Location during the Paleocene-Eocene of the two margins discussed in this article. (b) Paleogeography of the Lodo formation (California) during the late Paleocene to early early Eocene. (c) New Jersey margin sites.

[4] Despite an abundance of carbon isotope records, some uncertainty still surrounds the structure of the CIE. Both the magnitude of the CIE and the rate of change of $\delta^{13}C$ values during the initial excursion interval vary within and between marine and continental sections [*Koch et al.*, 1992; *Bowen et al.*, 2004; *Pagani et al.*, 2006a; *Schouten et al.*, 2007]. In continental sections, for example, the CIE tends to be a few per mil larger than recorded in marine sections (−5 to −6‰ versus −2.5 to −4.0‰), a feature that has been attributed in part to the effect of humidity and/or pCO_2 on terrestrial photosynthetic fractionation, but might also be a consequence of truncation of pelagic sections due to carbonate dissolution [*Bowen et al.*, 2004; *Zachos et al.*, 2005]. The latter may also contribute to the apparent abruptness of the onset of the CIE in pelagic sequences, which has been estimated to have occurred in less than 10 ka [*Röhl et al.*, 2000], but may have been more abrupt [*Thomas et al.*, 1999]. This particular deficiency with deep marine records is critical as it limits our ability to identify (with geochemical models) the rate and mass of carbon released and hence the source [*Pagani et al.*, 2006a]. Shallow marine sections, on the other hand, may more accurately record the marine CIE, in part because (1) shelf sediments lie well above the lysocline and should be largely unaffected by carbonate dissolution at the onset of the PETM and (2) overall sedimentation rates are substantially higher, though stratigraphic gaps may limit the continuity of these records.

[5] Another potentially key contribution from shallow marine records concerns the role of marine productivity and organic carbon deposition as a negative feedback at the PETM. Today shelf areas account for 80% of organic carbon accumulation and 30–50% of the total carbonate burial [*Ver et al.*, 1999]. Most pelagic sections are marked by low concentrations of organic matter in the CIE interval suggesting that an increase in organic carbon

burial was transient at most [*Bains et al.*, 2000]. On the shelf, many data, including dinoflagellate cyst (dinocyst) and nannofossil assemblages, indicate increased productivity during the CIE [*Bujak and Brinkhuis*, 1998; *Crouch et al.*, 2001; *Gibbs et al.*, 2006]. The global extent of this mechanism is less clear because organic carbon burial in most shelf areas, as well as on land, is insufficiently constrained to evaluate the link between environmental changes (higher temperatures and precipitation, lower oxygen levels, and elevated fluxes of sediments and dissolved ions) and global carbon fluxes. Specifically, did changes in carbonate and organic carbon burial on the shelf play a feedback role on ocean pH and pCO_2 at the PETM?

[6] The present study focuses on continental shelf locations to evaluate the character of regional impacts of the PETM on the coastal marine carbon cycle. Key objectives are to constrain the magnitude of the CIE on the shelf relative to the deep sea, and to document changes in mass accumulation rates of organic and inorganic carbon. To this end, we constructed high-resolution stable isotope, organic carbon and carbonate content records for coastal sections from the eastern and western margins of North America (Figure 1a). We expand on previous work on shallow marine Paleocene/Eocene (P/E) boundary sections along the New Jersey shelf, in the northwest Atlantic Ocean, and present new records from the Californian margin. The new data for the PETM interval in the Lodo Formation of California provided by this study represent the first such record for the eastern Pacific margin.

2. Paleogeographic and Geological Setting

[7] The east coast P-E sections, recovered in cores from the New Jersey Coastal Plain, include Ocean Drilling Program
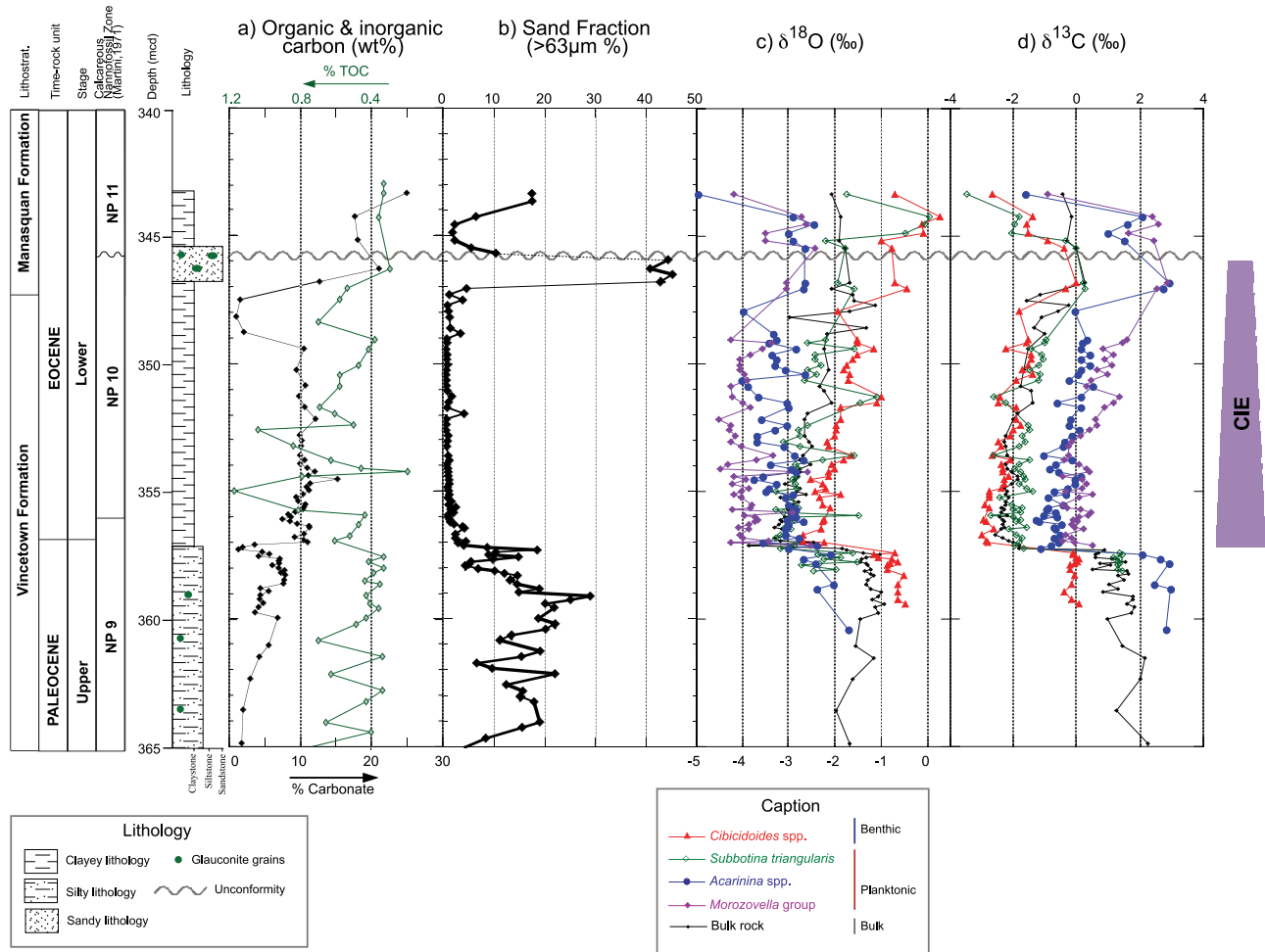
Figure 2. Results for the Bass River drill site. (a) Total organic carbon (TOC) and carbonate content (in wt %). Both data sets are plotted on the same vertical axis, but for better readability the horizontal axis for TOC has been inverted. The TOC data for Bass River are from *Cramer* [1999]. (b) Sand fraction (>63 μm) in wt %. (c) Oxygen isotope results for bulk rock and multispecimen benthic and planktonic foraminifers (values in per mil). (d) Carbon isotope results for bulk rock and benthic and planktonic foraminifers (values in per mil).

(ODP) Leg 174AX Site ''Bass River'' (39°36′42″N, 74°26′12″W) [*Miller et al.*, 1998b], and a U.S. Geological Survey site at Wilson Lake (39°39′21″N, 75°02′52″W) (Figure 1c). During the mid-to-late Paleocene, Bass River was located close to the shelf edge [*Miller et al.*, 2004]. Upper Paleocene sediments at this site are characterized by silty to sandy glauconite-rich sediments and finer-grained, clay-rich sediments just below the P/E boundary that extend into the lower Eocene (Figures 2a and 2b). A low-resolution (0.3−2 m sampling resolution) benthic fora-minifer carbon isotope record shows the base of the CIE coincident with the lithologic transition [*Cramer et al.*, 1999]. Additionally, published results from the Wilson Lake drill site, a nearshore equivalent to Bass River with similar lithologies, are included in our comparison [*Gibbs et al.*, 2006; *Zachos et al.*, 2006]. Previous work at Bass River and Wilson Lake has provided important strati-

graphic information as well as compelling evidence for environmental changes, including the CIE and SST anomalies [*Cramer et al.*, 1999; *Zachos et al.*, 2006], the presence of thick kaolinite-rich CIE layers [*Cramer et al.*, 1999; *Gibson et al.*, 2000], increased abundances of the dinocyst *Apectodinium* spp., pulses of freshwater tolerant taxa [*Sluijs et al.*, 2007], and transient nannoplankton pop-ulations indicative of increased biologic productivity [*Gibbs et al.*, 2006].

[8] The west coast P-E sections, Lodo Gulch (36°35′46″N/120°38′48″W) and Tumey Gulch (36°32′18″N/120° 38′29″W), are part of the Lodo Formation, exposed in the Panoche Hills in the Central Valley of California (Fresno County, Figure 1b). The ''Lodo Gulch'' is the type section of the Lodo Formation [*White*, 1938; *Martin*, 1943]. The section comprises 350 m of siltstone with rare thin (meter scale or less) sand layers deposited in a neritic-

bathyal setting (shallower than 200 m), overlain by bathyal deposits in the middle of the section (~600 m water depth, middle Eocene) [*Berggren and Aubert*, 1983]. The Tumey Gulch section is located about 6 km SE of Lodo Gulch. At this locality the Lodo Formation is 1000 m thick, and the sediments were deposited in a bathyal environment located on the shelf edge or upper continental slope [*Martin*, 1943; *Berggren and Aubert*, 1983; *Bartow*, 1991] (see Figure 1c). Although the California margin was tectonically active through the Paleogene, the Panoche Hills are located east of the San Andreas fault, so the sections have not migrated significantly in the last 55 Ma [*Engebretson et al.*, 1985].

3. Methods
3.1. Analytical Methods

[9] The Bass River cores were sampled at 6 to 50 cm intervals over 25 m, while the Lodo and Tumey Gulch sections were sampled at 2 to 50 cm intervals over 80 and 60 m, respectively. Sampling resolution was highest near the P/E boundary. Samples were washed over a 63 μm sieve, and the sand fraction was determined (weight percent (wt %) of both siliciclastic and carbonate grains >63 μm). Stable isotope analyses were performed on bulk sediment, foraminifer shells (picked in the 180–250 μm fraction), and bulk organic matter.

[10] Stable isotope analyses on carbonate material were performed at the University of California at Santa Cruz (UCSC), using a Micromass Optima mass spectrometer for bulk carbonates and a Micromass Prism mass spectrometer for foraminifers analyses (in general, between 3 and 6 pristine specimens were combined for each analysis, though some single foraminifer analysis were done at Bass River). The carbon isotope ratio of bulk organic matter ($\delta^{13}C_{org}$) was measured for a subset of samples following procedures described by *Harris et al.* [2001]. Using this method, decarbonated samples were analyzed at UC Davis on a Europa 20-20 continuous flow isotope ratio mass spectrometer following combustion at 1000°C in a Europa ANCA-GSL CN analyzer. Stable isotope values are reported in the δ (per mil) notation relative to the Vienna Pee Dee belemnite standard (VPDB). External analytical precision based on replicate analysis of two standards (NBS19 and Carrara Marble) was better than 0.10 and 0.05‰ for O and C isotopes, respectively. Paleowater temperatures were estimated using $\delta^{18}O_{Foraminifer}$ and standard calibration equations for *Cibicidoides* spp. [*Shackleton*, 1974] and mixed layer planktonic foraminifera [*Bemis et al.*, 1998], considering a Paleogene $\delta^{18}O_{seawater}$ of 0.5‰.

[11] Total inorganic carbon content (TIC) (converted to percent $CaCO_3$) was determined at UCSC on a UIC Coulometer (model 5012), with a precision better than ±0.5% $CaCO_3$. Total carbon (TC) and total nitrogen (TN) for the Lodo Gulch and Tumey Gulch sections were measured at UCSC on a CarloErba CHNS analyzer, with a standard deviation (1σ) of 0.01% for TN and 0.02% for TC. Total organic carbon (TOC) was calculated by subtracting TIC from TC. C:N molar ratios were calculated using TOC and TN corrected for the molar weight of C and N, respectively.

[12] For discussion and comparison, we used published TOC data at Bass River [*Cramer*, 1999], and published calcareous nannofossil biostratigraphy, TOC, percent $CaCO_3$ and stable isotope data at Wilson Lake [*Quattlebaum*, 2004; *Gibbs et al.*, 2006; *Zachos et al.*, 2006].

3.2. Age Models, Linear Sedimentation Rates, and Mass Accumulation Rates

[13] Age models used to constrain the broad stratigraphy of the Lodo Gulch, Tumey Gulch and Bass River sections are mainly based on the first (FOs) and last (LOs) occurrences of calcareous nannofossil bioevents using the zonation of *Martini* [1971, Plates 1–4, Tables 1–6] with modifications from *Perch-Nielsen* [1985]. Additionally, the LO of the planktonic foraminifer *Morozovella velascoensis* was used as a marker for the top of zone P5 at 54.7 Ma [*Berggren et al.*, 1995; *Kelly et al.*, 2001]. Previous work on paleomagnetic [*Cramer et al.*, 1999] and organic dinocysts data, such as the presence of *Apectodinium augustum* [*Bujak and Brinkhuis*, 1998; *Crouch et al.*, 2003] were also integrated. The age model for the CIE interval (in thousand of years (ka) post onset of the CIE) was determined by approximately correlating the continental margin $\delta^{13}C$ records to the orbital age model for the $\delta^{13}C$ record at ODP Site 690 using the age model from *Röhl et al.* [2000].

[14] Linear mass accumulation rates (MARs (in g cm^{-2} ka^{-1})) are calculated using linear sedimentation rate (in cm^2 ka^{-1}), percent $CaCO_3$ or percent TOC data (for MAR$_{Carbonate}$ or MAR$_{Organic\ carbon}$, respectively), and synthetic dry bulk density data (in g cm^{-3}). The latter was necessary because no dry bulk density data exists for the sections investigated in this study. These are derived (including at Wilson Lake) by using porosity estimates from the empirical curves of *Bryant et al.* [1981] and a grain density of 2.65. The "sand" calibration curve was used to estimate porosity for samples with >15 wt % sand fraction, while two porosity estimates were derived for samples with <15 wt % sand fraction, one based on the "silt" curve and one based on the "clay" curve. This results in a range of possible mass accumulation rates (represented graphically by error bars) for samples characterized by the silt-rich and clay-rich lithologies. Comparing the synthetic density estimates for the Bass River and Wilson Lake sections and measured bulk densities on similar lithologies at equivalent burial depth on the New Jersey margin (ODP Leg 150 [*Mountain et al.*, 1994]) suggest that the densities obtained for this study are robust.

[15] Excess cumulative mass accumulation (in g cm^{-2}) at time "t" is defined as the cumulative mass per cm^2 deposited in excess of Upper Paleocene rates between the onset of the CIE and "t."

4. Results
4.1. Biostratigraphy

[16] The primary biostratigraphic datums identified at Bass River (Figure 2) are the NP9–NP10 boundary at 356.95 m below surface (mbs) (FO of *Rhomboaster bramlettei*) and the NP10–NP11 boundary coinciding with a
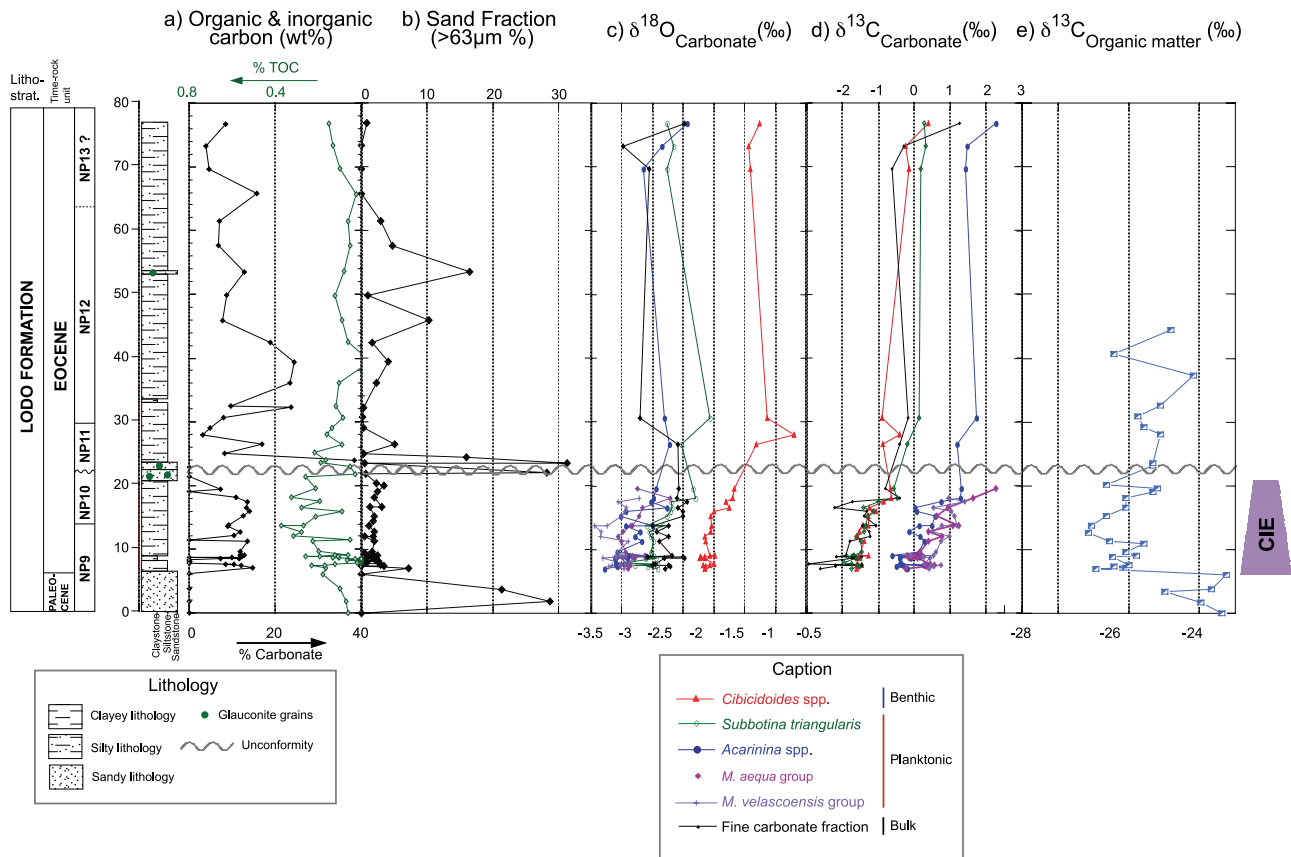
Figure 3. Results for the Lodo Gulch section. (a) Total organic carbon (TOC) and carbonate content (in wt %). (b) Sand fraction (>63 μm) in wt %. (c) Oxygen isotope results for bulk fine carbonate fraction and benthic and planktonic foraminifers (values in per mil). (d) Carbon isotope results for bulk rock and benthic and planktonic foraminifers (values in per mil). (e) Carbon isotope results for bulk organic matter (values in per mil).

disconformity at 345.92 mbs (marked by the simultaneous FOs of *Tribrachiatus orthostylus* and *Discoaster diastypus* and LO *Fasciculithus* spp.). At Lodo Gulch (Figure 3), the main biostratigraphic datums identified are the NP9–NP10 boundary at 14.40 m, the NP10–NP11 boundary at 23.50 m, and the NP11–NP12 boundary 30.70 m (FOs of *R. bramlettei*, *T. orthostylus,* and *D. lodoensis* respectively). We suspect the presence of a disconformity between 20.30 and 23.50 m based on the simultaneous FOs of *D. diastypus*, *D. kuepperi* and *T. orthostylus* and the LO of the genus *Fasciculithus* at this stratigraphic level. At Tumey Gulch (Figure 4), a diverse *Fasciculithus* spp. assemblage at 27.40 m suggests a correlation to Zone NP9 for the base of the section. The NP9/NP10 zonal boundary is tentatively assigned at 37.86 m (FO of the genus *Rhomboaster*). As in the Lodo Gulch section, the FOs of *D. diastypus*, *D. kuepperi* and *T. orthostylus* occur simultaneously at 51.21 m as well as the FO of *Sphenolithus radians* indicating a disconformity at the top of the NP10 zone. At 62.92 m, the FO of *D. lodoensis* indicates the NP11/NP12 boundary.

4.2. CIE Interval on the New Jersey Margin: Bass River Drill Site

[17] The foraminifer and bulk carbonate $\delta^{18}O$ and $\delta^{13}C$ records at Bass River (Figures 2c and 2d) are characterized by uniform values in the upper Paleocene prior to an abrupt negative shift at 357.2 mbs (the onset of the "CIE"). Single-specimen foraminifer data (Figure 5) also show an abrupt negative shift at the CIE, with essentially no transitional $\delta^{13}C$ values occurring in the *Subbotina*, *Acarinina*, or *Morozovella* records. The average amplitude of the CIE is 2.7‰ in benthic foraminifers and 3.3–3.4‰ in planktonic foraminifers, but it is as large as 4.3‰ in *Acarinina* spp. (Table 1). Oxygen isotope ratios decrease by 1.6‰ in benthic foraminifers and by 0.5–1.3‰ in planktonic foraminifers, with *Morozovella* showing the largest decrease (Table 2). The $\delta^{13}C$ values of single specimen *Acarinina* and *Morozovella* within a single sample are fairly constant, but $\delta^{18}O$ show a wider spread of values. It is not clear if this is due to seasonal changes in temperature or salinity recorded by single specimens, whether it is linked to preservation of the foraminifers, or if this reflects a large range of $\delta^{18}O$ values within the sample population.
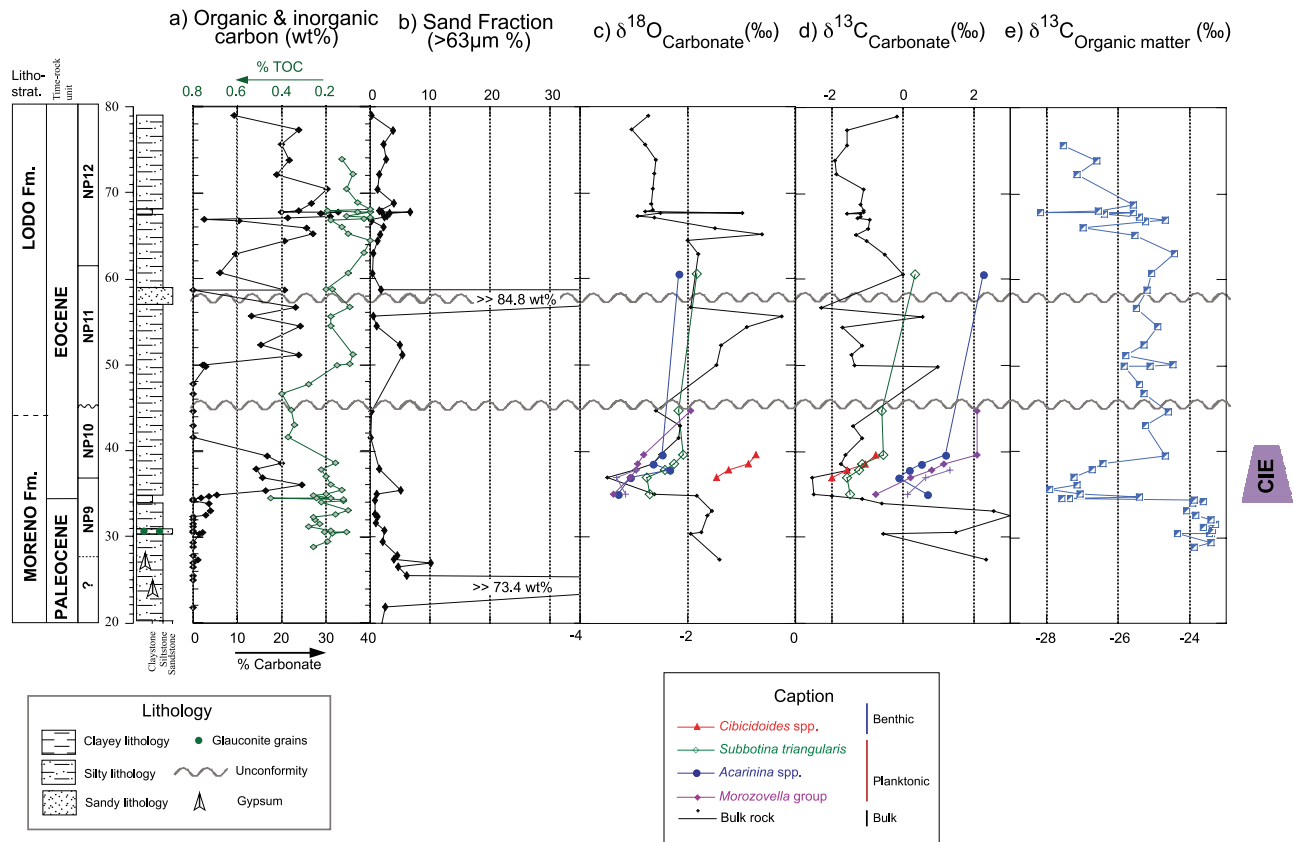
Figure 4. Results for the Tumey Gulch section. (a) Total organic carbon (TOC) and carbonate content (in wt %). (b) Sand fraction (>63 μm) in wt %. (c) Oxygen isotope results for bulk rock and benthic and planktonic foraminifers (values in per mil). (d) Carbon isotope results for bulk rock and benthic and planktonic foraminifers (values in per mil). (e) Carbon isotope results for bulk organic matter (values in per mil).

[18] Calculation of sea surface temperatures (SSTs) using the $\delta^{18}O$ values of surface-dwelling *Acarinina* spp. yields temperature estimates of 26°C prior to the CIE, and *Acarinina* spp. and *Morozovella* spp. $\delta^{18}O$ values indicate SSTs of 30°C–31°C at the peak of the event (Table 3). These temperatures agree with those determined by TEX$_{86}$ analyses [*Sluijs et al.*, 2007], a method based on the distribution of crenarchaeotal tetraether lipids [*Schouten et al.*, 2002]. The relatively good agreement between the TEX$_{86}$ and oxygen isotope temperature estimates indicate that variations in salinity on the foraminifer $\delta^{18}O$ values were negligible at Bass River. Multiple and single specimen analyses of thermocline-dwelling *Subbotina* spp. (Figures 2 and 5 and Table 1) show an average change in $\delta^{18}O$ of 1.3–1.5‰ at the CIE, corresponding to 6°C–7°C of warming (from 23°C to 30°C). On the basis of *Cibicidoides* spp. $\delta^{18}O$ values, benthic water temperatures are estimated to have warmed from 19°C pre-CIE to 23°C during the CIE. Using *Acarinina* spp. data (pre-CIE), *Morozovella* spp. data (post CIE), and *Cibicidoides* spp. data, the temperature gradient from the surface to the seafloor at Bass River is

estimated between 7°C and 8°C through the late Paleocene to Early Eocene. The ~1°C difference between the *Morozovella* and *Acarinina* spp. $\delta^{18}O$ records probably reflects a difference in the depth habitats of each foraminifer group.

[19] The onset of the CIE at Bass River corresponds to a change in lithology from siltstones with glauconite below the CIE to claystones above (Figure 2). Sand fraction decreases from 7.0 to 29.0 wt % below the CIE to <1.0 wt % above, and percent CaCO$_3$ increases slightly from 7.0 wt % to 11.0 wt % (Figure 2). TOC averages 0.5–0.6 wt % throughout the section (values from *Cramer* [1999]), and does not increase markedly at the onset of the CIE (Figure 2a). Two discrete intervals with high TOC (up to 1.2 wt %) occur at 2.5 m and 5.0 m above the onset of the event. TOC shows a steady decrease up section from 352.7 mbs [*Cramer*, 1999], through the CIE recovery interval, and carbonate content decreases at 349.4 mbs (from ~10 to 3.0 wt %). A glauconite-rich sandstone interval truncates the end of the recovery at 346.8–345.9 mbs (Figure 2).
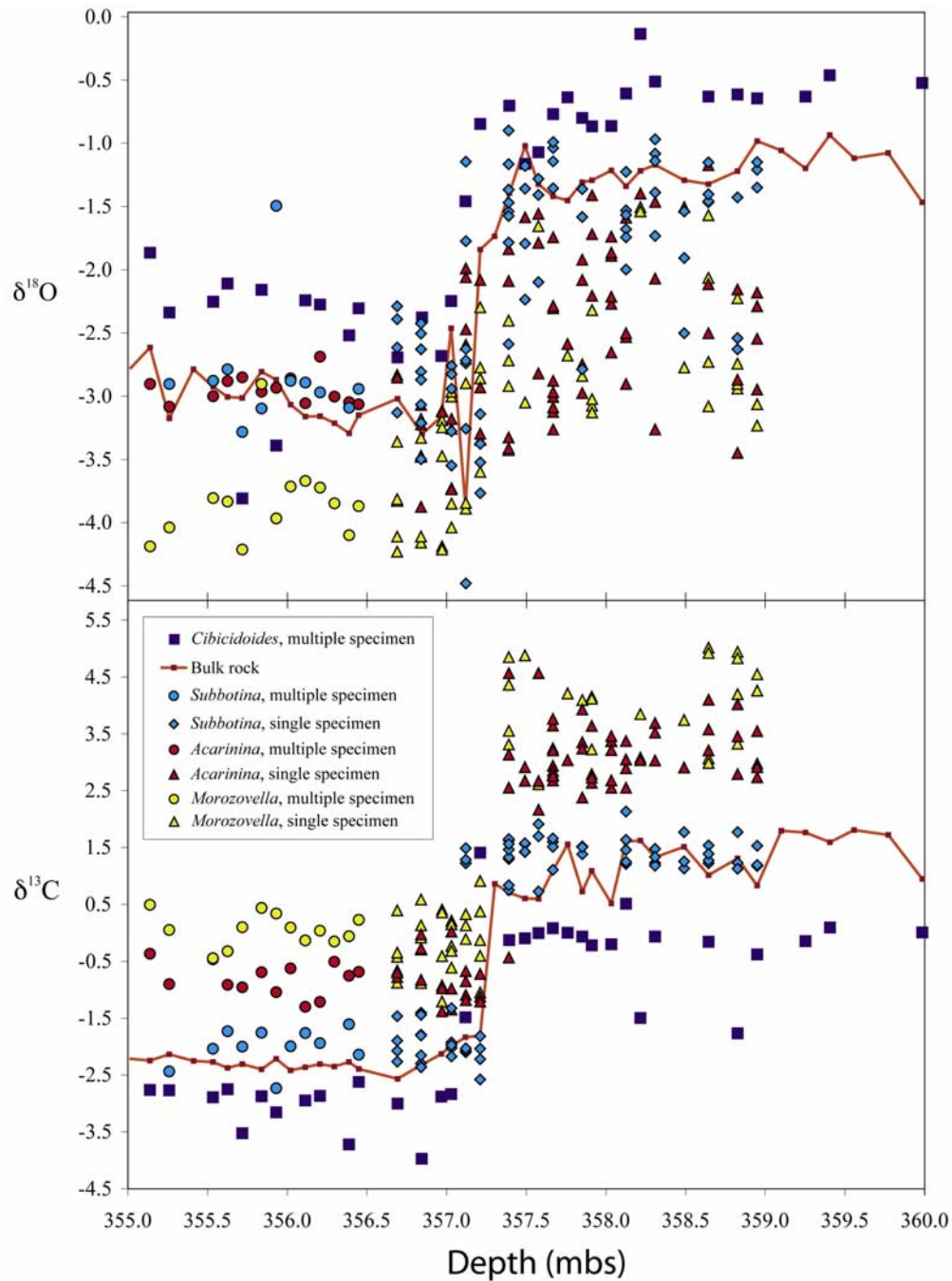
Figure 5. Single-specimen analysis of planktonic foraminifers from Bass River (values in per mil).

4.3. CIE Interval on the Californian Margin

4.3.1. Lodo Gulch Section

[20] Lithologies at the base of the Lodo Gulch section (0–6.1 m) are characterized by sandstones (20–30% sand fraction) and the absence of carbonate (<0.1% carbonate, Figure 3). At 6.1 m, grain size decreases abruptly (<5 wt % sand fraction), percent $CaCO_3$ increases (13.0–15.0 wt %), TOC increases slightly (from <0.1 to 0.3%), and the dominant lithology is siltstone. Between 6.1 and 19.9 m, well-preserved foraminifera are relatively common, especially in layers with high clay content. The lowest $\delta^{13}C$ and $\delta^{18}O$ values for all foraminifer species are recorded at the 6.1 m stratigraphic level (see Tables 2 and 3, "CIE values"). At the same level, $\delta^{13}C_{org}$ (Figure 3e) abruptly decrease from a mean of −23.9‰ near the base of the section to −27.1‰ (onset of the "CIE"). Although $\delta^{13}C_{org}$ could be influenced by contributions of terrestrial organic matter, the absence of terrestrial palynomorphs, the relatively high $\delta^{13}C_{org}$ values and the low C:N ratios (Figure 6) around the CIE interval indicate that the

Table 1. Oxygen Isotope Values at Bass River, Lodo Gulch, and Tumey Gulch Before and After the CIE[a]

	Preexcursion $\delta^{18}O$ Versus PDB, ‰			Postexcursion $\delta^{18}O$ Versus PDB, ‰			Amplitude of $\delta^{18}O$ Change Versus PDB, ‰		
	Maximum	Average	T Average, °C	Maximum	Average	T Average, °C	Maximum	Average	Average Temperature Change, °C
				Bass River Section					
Bulk carbonate	1.55	0.91		−3.87	−3.20		5.42	**4.11**	
Cibicidoides spp.	−0.64	−0.89	**19**	−2.04	−1.82	**23**	1.40	**0.93**	**4**
Subbotina spp.	−1.51	−1.91	**23**	−3.51	−3.22	**30**	2.00	**1.31**	**7**
Morozovella spp.	-	-		−4.24	−3.55	**31**	-	-	
Acarinina spp.	−2.68	−2.38	**26**	−3.56	−3.31	**30**	0.88	**0.93**	**4**
Vertical Gradient			**7**			**8**			
				Lodo Gulch Section					
Bulk carbonate	-	-		−2.46	−2.34		-	-	
Cibicidoides spp.	-	-		−1.68	−1.60	**22**	-	-	
Subbotina triangularis	-	-		−2.78	−2.54	**26**	-	-	
Morozovella aequa group	-	-		−3.02	−2.92	**28**	-	-	
Morozovella velascoensis	-	-		−3.21	−3.06	**29**	-	-	
Acarinina spp.	-	-		−3.28	−3.09	**29**	-	-	
Vertical Gradient						**7**			
				Tumey Gulch Section					
Bulk carbonate	−2.15	−2.49		−3.49	−3.05		1.34	0.56	
Cibicidoides spp.	-	-		−1.47	−1.35	**21**	-	-	
Subbotina triangularis	-	-		−2.75	−2.73	**27**	-	-	
Morozovella aequa group	-	-		−3.37	-		-	-	
Morozovella velascoensis	-	-		−3.31	-		-	-	
Acarinina spp.	-	-		−3.30	-				

[a]Values are based on a five-point running average. Temperatures for benthic foraminifers were estimated using the equation of *Shackleton* [1974], and temperatures for planktonic isotopes were based on the low-light *Orbulina universa* equation described by *Bemis et al.* [1998] (see text for details). Boldface indicates that data are from multiple locations; average values are used in text discussion.

composition of the organic matter did not change through the event, and was mostly of marine origin. At the peak of the PETM warming ("peak CIE"), $\delta^{18}O$-based SST at Lodo Gulch ranges between 28°C and 29°C, and seafloor water temperature is 22°C. Thus, the Early Eocene vertical temperature gradient in the water column at Lodo Gulch is similar to the gradient at Bass River, about 7°C based on *Morozovella* spp. and *Cibicidoides* spp. $\delta^{18}O$ data.

[21] In the Lodo Gulch section, both $\delta^{13}C$ and $\delta^{18}O$ increase between 6.1 and 19.90 m (within the CIE "recovery" interval, Figure 3e). C:N ratios increase 4 m above the onset of the CIE, within the recovery interval, indicating a possible increase in terrigenous organic matter supply ~40–60 ka after the onset of the event (Figure 6). The increase in terrigenous organic matter is not paralleled by noticeably more negative values in $\delta^{13}C_{org}$, and, thus, the terrestrial component is probably minor even in this interval. The $\delta^{13}C_{Foraminifer}$ record above 19.9 m contains several gaps where well-preserved foraminifers could not be found. A glauconite-rich sand bed between 20.8 and 23.8 m truncates the recovery interval.

4.3.2. Tumey Gulch Section

[22] The lithologies in the Tumey Gulch section (Figure 4) are dominated throughout by siltstones (3–10 wt % sand fraction). Carbonate is generally absent from the base of the section to 34.6 m, with the exception of a 10-cm thick glauconitic bed at 30.4 m (~2.0 wt % carbonate) and a 35-cm bed at 32.6 m (4.1 wt % carbonate). Foraminifers are absent in these carbonate-rich beds and preservation of the carbonate is poor (e.g., dolomite rhombs are visible in smear slides). Thus the bulk carbonate stable isotope

record in this interval could be skewed significantly by the presence of authigenic carbonate (Tables 1 and 2 and Figure 4). The most prominent changes occur at 34.5 m, where carbonate content increases up section, bulk carbonate

Table 2. Estimates of Sedimentation Rates and Average MARs for Different Intervals Within the CIE[a]

	Sedimentation Rate, cm ka^{-1}	MAR Carbonate, g cm^{-2} ka^{-1}	MAR Organic Carbon, g cm^{-2} ka^{-1}
	Bass River		
Pre-CIE	2.5	0.16	0.01
Onset	NA	NA	NA
Peak CIE	11.9	1.86	0.12
Recovery	11.9	0.33	0.08
	Wilson Lake[b]		
Pre-CIE	8.4	0.04	0.01
Onset	6.8	0.06	0.02
Peak CIE	19.5	1.02	0.07
Recovery	19.5	1.24	0.11
	Lodo Gulch		
Pre-CIE	1.5	0.00	0.00
Onset	NA	NA	NA
Peak CIE	16.8	2.63	0.06
Recovery	24.6	2.42	0.03
	Tumey Gulch		
Pre-CIE	1.5	0.02	0.01
Onset	NA	NA	NA
Peak CIE	7.3	1.31	0.02
Recovery	3.3	0.32	0.02

[a]Values are derived by correlating the continental margin sites to ODP Site 690 using the age model from *Röhl et al.* [2000]. NA indicates not applicable.
[b]Data from *Quattlebaum* [2004].

Table 3. Carbon Isotope Values at Bass River, Lodo Gulch, and Tumey Gulch Before and After the Carbon Isotope Excursion[a]

Species	Preexcursion δ^{13}C Versus PDB, ‰		Postexcursion δ^{13}C Versus PDB, ‰		Amplitude of δ^{13}C Change Versus PDB, ‰	
	Maximum	Average	Maximum	Average	Maximum	Average[b]
Bass River Section						
Bulk carbonate	1.79	1.21	−2.56	−2.25	4.35	**3.46**
Cibicidoides spp.	0.09	−0.1	−3.00	−2.84	3.09	**2.74**
Subbotina spp.	1.46	1.34	−2.14	−1.91	3.6	**3.25**
Morozovella spp.	-	-	−0.46	0.00	-	-
Acarinina spp.	2.95	2.6	−1.30	−0.83	4.25	**3.43**
Lodo Gulch Section						
Bulk carbonate	-	-	−2.95	−2.29	-	-
Bulk organic matter	−23.26	−23.86	−27.13	−27.10	3.87	**3.24**
Cibicidoides spp.	-	-	−1.58	−1.57	-	-
Subbotina triangularis	-	-	−1.76	−1.62	-	-
Morozovella aequa group	-	-	−0.25	0.28	-	-
Morozovella velascoensis	-	-	0.28	0.48	-	-
Acarinina spp.	-	-	−0.51	−0.23	-	-
Tumley Gulch Section						
Bulk carbonate	3.02	2.33	−2.52	−1.73	5.54	4.06
Bulk organic matter	−23.27	−23.69	−27.54	−27.09	4.27	**3.4**
Cibicidoides spp.	-	-	−1.99	-	-	-
Subbotina triangularis	-	-	−1.56	−1.52	-	-
Morozovella aequa group	-	-	−0.78	-	-	-
Morozovella velascoensis	-	-	0.13	-	-	-
Acarinina spp.	-	-	−0.11	-	-	-

[a]Values are based on a five-point running average.
[b]Boldface indicates that data are from multiple locations.

δ^{13}C and δ^{18}O values decrease by 4.1‰ and 0.6‰, respectively, and δ^{13}C$_{org}$ decreases by 3.4‰ (i.e., at the onset of the "CIE"). As at Lodo Gulch, the organic matter across the CIE appears to be dominantly marine with a low C:N ratio (Figure 6). Between 34.2 and 34.5 m, the lithology is a reddish fine-silt layer (<0.9% sand fraction, <0.1% CaCO$_3$).

[23] The first well-preserved foraminifers above the base of the section are found at 35.0 m, coincident with a sharp increase in percent CaCO$_3$ (up to 16.4 wt %). The low δ^{13}C and δ^{18}O values measured from foraminifers at this level confirm a peak CIE stratigraphic assignment. In this interval, benthic foraminifer δ^{13}C and δ^{18}O values are −2.0‰, and planktonic foraminifer values range from 0.11 to −1.6‰ for δ^{13}C and from −2.7‰ to −3.4‰ for δ^{18}O, depending on the taxon analyzed (Tables 1 and 2). These values are similar to equivalent intervals at Lodo Gulch (Tables 2 and 3), and indicate peak SSTs of 27°C and seafloor water temperatures of 21°C during the CIE. As at Lodo Gulch, C:N ratio increase 4 m above the onset of the CIE (Figure 6), indicating a possible increased contribution of terrigenous organic matter in this interval.

[24] Immediately above 35.0 m within the Tumey Gulch section, both δ^{13}C$_{org}$ and δ^{13}C$_{carbonate}$ gradually increase through the section to 35.0 m (within the CIE "recovery" interval). At 41.6 m, carbonate content decreases to <0.1wt % and remains low until 49.9 m, above which it fluctuates around 20 wt %. Organic matter content at Tumey Gulch (Figure 4a) is relatively constant (~0.2 wt %) from the pre-CIE interval throughout the recovery phase, and increases up to 0.4 wt % above 39.5 m (with the post-

CIE recovery interval). Sediments above the disconformity are characterized by <0.2 wt % TOC.

4.4. Sedimentation Rates and Mass Accumulation Rates

[25] We correlated the continental margin sections with the reference deep sea section at Site 690 based on tie points at the last pre-CIE values, and peak CIE values (in Figure 7). This results in an inferred "time gap" of 20–23 ka at Bass River, Lodo Gulch and Tumey Gulch. Because the onset of the CIE in pelagic bulk δ^{13}C records might be altered by dissolution and bioturbation [Zachos et al., 2005, 2007], this gap is likely an artifact (see discussion below). Regardless, sedimentation rates for the peak CIE and recovery intervals should not be significantly affected by this small uncertainty. We estimate continuous sedimentation during the onset of the CIE at Wilson Lake (6.8 cm ka^{-1}, Table 2). During peak CIE, sedimentation rates range from 7.3 cm ka^{-1} (Tumey Gulch) to 19.5 cm ka^{-1} (Wilson Lake, Table 2). Sedimentation rates during the recovery are difficult to estimate because of the numerous unconformities, but must be very high. At Lodo Gulch, the relatively long recovery interval can be correlated to the ODP Site 690 record (see Figure 7) yielding a sedimentation rate of 24.6 cm ka^{-1}. For Bass River and Wilson Lake, assuming sedimentation rates similar to peak CIE yield a good fit to the ODP Site 690 record. Tumey Gulch is the only section where sedimentation rates are interpreted to have decreased during the recovery interval (from 7.3 cm ka^{-1} to 3.3 cm ka^{-1}). On the basis of biostratigraphic data, Upper Paleocene sedimentation rates at Bass River are estimated
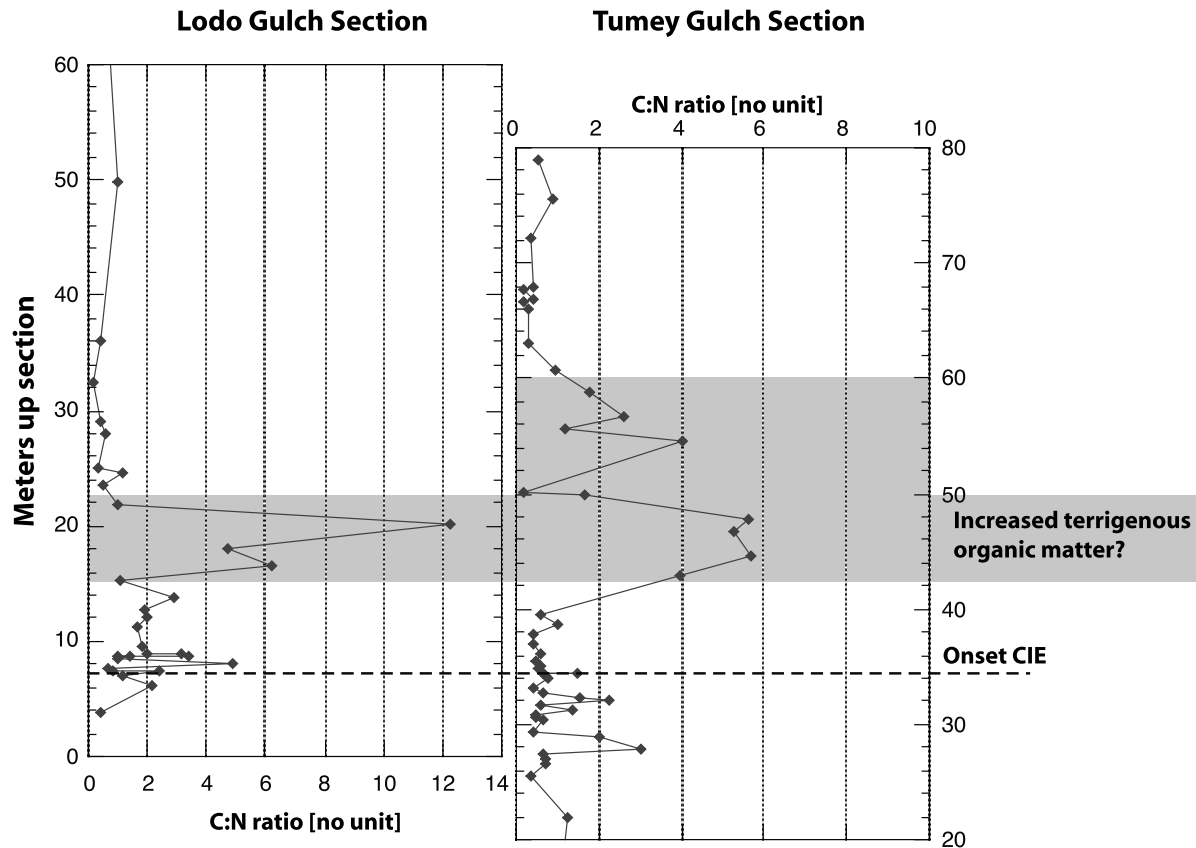
Figure 6. C:N ratio at Lodo Gulch and Tumey Gulch. The grayed zone represents an interval of higher C:N ratio where the contribution of terrigenous organic matter is potentially higher.

to be 2.7 ± 0.6 cm ka^{-1} [*Cramer*, 1999] and range from ~ 1 to 2 cm ka^{-1} in the Lodo Formation. Thus, sedimentation rates increased by an order of magnitude across the CIE (Tables 2 and 4).

5. Discussion

5.1. Implication of the Shelf Record for the Magnitude and Timing of the CIE

[26] The shelf records indicate that the average amplitude of the CIE on the continental margins (2.8−3.5‰) is closer to deep-sea records (2.5−3.0‰) than terrestrial records (∼5‰). The amplitude of the CIE is similar on both margins of North America, whether it is measured on bulk organic matter or foraminiferal calcite (Table 3). The consistency in δ^{13}C between geographical shelf locations and sample materials suggests that the full amplitude of the CIE is captured on the shelf. This magnitude is lower by ∼2‰ relative to terrigenous records, and we concur with others [*Bowen et al.*, 2004] that this probably indicates an amplification of the CIE in many terrigenous records though the reasons remain unclear. One possibility is that carbon fractionation during photosynthesis is a phenomenon highly species-specific, yielding a wide range of excursion values at the P/E boundary that depend on the organic compound analyzed [*Schouten et al.*, 2007].

[27] The temperature increase at the CIE in both surface and deeper waters on the shelf (5°C−6°C) based on the

oxygen isotopes is slightly less pronounced than based on TEX$_{86}$ [*Sluijs et al.*, 2007]. The estimates are both generally consistent with estimated SST and deepwater warming during the PETM [*Thomas and Shackleton*, 1996; *Zachos et al.*, 2001; *Tripati and Elderfield*, 2005]. Interestingly, surface, thermocline and bottom water temperatures warmed by a similar magnitude at Bass River during the PETM (Table 3). The foraminifer stable isotope records show interspecies gradients that are very similar to patterns observed in deep-sea sections (Figures 2). For example, species of the genus *Morozovella* that largely resided in the mixed layer [*D'Hondt et al.*, 1994], yield the highest δ^{13}C and lowest δ^{18}O values, and the benthic foraminifer *Cibicidoides* yield the lowest δ^{13}C and highest δ^{18}O values, respectively.

[28] The amplitude of the CIE on the shelf is most comparable with the open ocean record at ODP Site 690 (Weddell Sea). The isotopic composition of dissolved carbon (δ^{13}C$_{DIC}$) in mixed layer waters between the New Jersey margin and the Weddell Sea were likely similar, as single-specimen *Morozovella* from both locations show essentially the same range of preexcursion and excursion δ^{13}C values [*Zachos et al.*, 2007]. The same appears to be true for the initial Eocene CIE δ^{13}C values from Lodo Gulch and Tumey Gulch sections, which are essentially identical to those from Maud Rise and New Jersey. Species living deeper in the water column do not show a similar pattern.
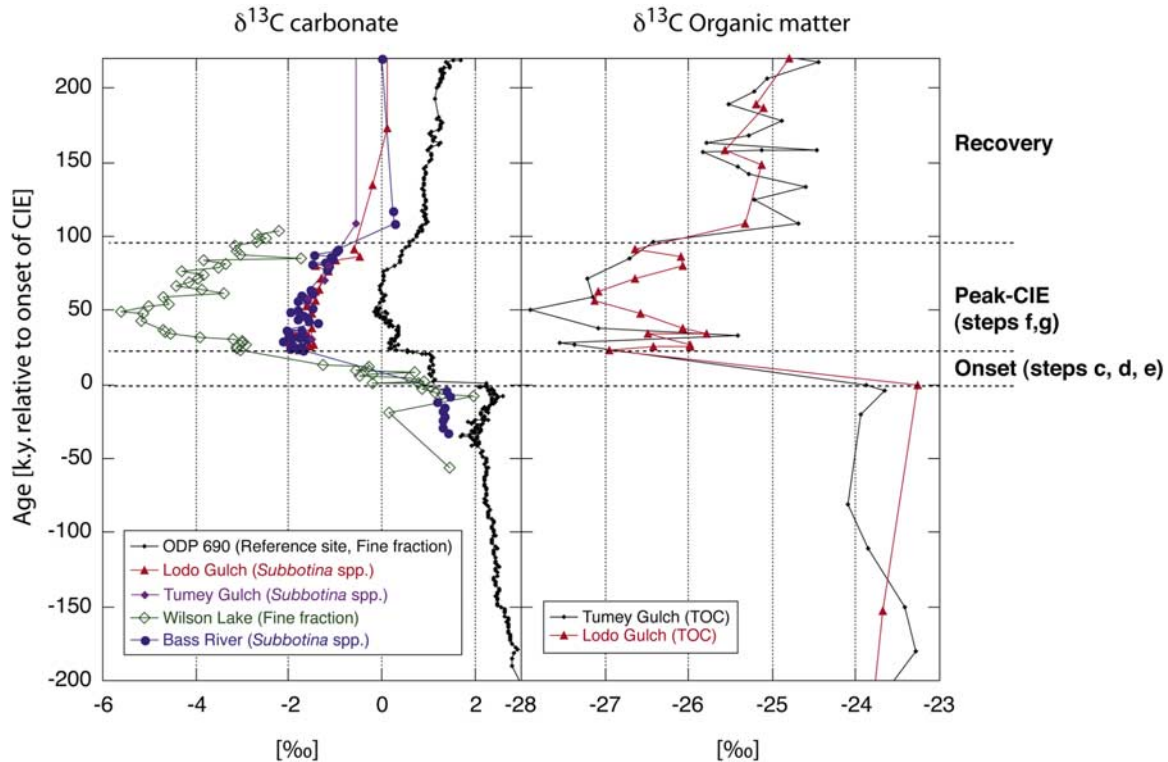
Figure 7. Shelf carbon isotope values across the CIE correlated to ODP Site 690 plotted using the age model of *Röhl et al.* [2000]. Correlations were done using Analyseries 2.0 [*Paillard et al.*, 1996].

For example, *Subbotina* spp. (Figure 8) from Bass River yield similar pre-CIE $\delta^{13}C$ values to those from ODP Site 690 (median $\delta^{13}C$ values are 1.4 and 1.6‰, respectively), but are about 1.3‰ lighter during the CIE (median $\delta^{13}C$ values are −2.0 and −0.6‰, respectively). This difference is as yet unexplained, but could indicate a change in thermocline structure, vertical organic carbon fluxes, and/or a change in the depth habitat of *Subbotina* spp. at either ODP Site 690 or Bass River.

[29] Compared to other open ocean sites, for example, DSDP Sites 527, 577, 557, and ODP Site 1209, the peak CIE $\delta^{13}C$ values of carbonate from both the New Jersey sections and Site 690 are lower, and therefore the magnitude of the CIE is larger. It is possible that these carbon isotope differences reflect on local variations associated with vertical mixing or export production. In theory, a reduction in export productivity and organic carbon burial should lower local DIC $\delta^{13}C$. An alternative explanation for the somewhat increased magnitude of the CIE on the shelf is that the early Eocene portion of the pelagic record was truncated by dissolution, and are thus less complete than the continental margin records.

[30] Carbon isotope data immediately above and below the P/E boundary at Bass River suggest an abrupt onset of the CIE, that is, two distinct populations of data are apparent on a $\delta^{18}O$ versus $\delta^{13}C$ crossplot of single specimen planktonic foraminifer (Figure 8): a pre-CIE population and a

CIE population. A similar pattern is also observed within the $\delta^{13}C_{org}$ records at Lodo Gulch and Tumey Gulch (Figures 3 and 4). In pelagic sections, the relatively rapid step in $\delta^{13}C$ is thought to be partly an artifact of the intense dissolution, loss of carbonate and reworking [*Zachos et al.*, 2005, 2007]. On the shelf, carbonate dissolution is unlikely to result from lysocline shoaling and most likely does not account for the rapid shift observed in $\delta^{13}C_{org}$. One possible explanation is that the onset of the event transpired over an interval equal to or shorter than the sampling resolution of our study (ranging from 1 to 4 ka). Sediment mixing by bioturbation could also mask intermediate $\delta^{13}C$ values in multispecimen analysis. However, single-specimen analyses (Figure 5) show no intermediate values around the CIE interval, prompting us to dismiss this possibility, at least for the Bass River site. An alternative explanation is that the North American shelf $\delta^{13}C$ records do not capture the initial ~23 ka of the CIE. Some continental margin records [e.g., *Lu et al.*, 1998; *Crouch et al.*, 2003] show a gradual decrease in $\delta^{13}C_{\text{bulk carbonate}}$ or $\delta^{13}C_{org}$ values, which may argue for a truncation of our records. However, in other expanded continental records such as sections in the pre-Alps [*Giusberti et al.*, 2007] the onset of the CIE is instantaneous with no evidence for a hiatus. On this basis, *Giusberti et al.* [2007] proposed that the CIE happened in a geologic instant, and that the stepwise increase in the fine-fraction $\delta^{13}C$ record at ODP Site 690

Table 4. Compilation of Continental Shelf and Slope Data for the PETM Interval[a]

	Tethys Ocean — Northern				Tethys Ocean — Southern				Pacific Ocean — South		Pacific Ocean — North			North Atlantic Ocean		
	Alamedilla (Spain)	Aktumsuk, Uzbekistan	Kaurtakapy, Kazakhstan	Elles Section, Tunisia	Abu Zenima, Egypt	Zomet Telalim, Israel	Gebel Duwi, Egypt	Gebel Matulla, Egypt	Tawanui, New Zealand	Tumey Gulch, California	Lodo Gulch, California	Wilson Lake, New Jersey	Bass River, New Jersey	Trabakua Pass, Spain	Zumaia, Spain	Ermua, Spain
Paleoenvironment/ water depth	basin	shallow neritic	shallow neritic	slope shelf (~100 m)	500 m	500– 700 m	75– 100 m	500 m	shelf	slope	shelf	shelf	shelf	basin- slope	1000 m	basin- slope
Sed rate pre CIE[b]	0.4	0.3	0.3	0.6	0.2	0.2	0.1	0.2	8.5	1.9	0.9	8.4	2.7	0.8	1.6	3
Sed rate during CIE[c]	1.8	1.9	1.3	3.0	0.1	0.6	0.8	0.6	1.5	7.3	16.8	19.9	11.9	2.7	2.7	14
Sed rate ratio[d]	4.2	6.3	4.3	5.0	0.5	3.0	8.0	3.0	0.2	3.8	18.7	2.4	4.4	3.4	1.7	4.7
Carbonate pre-CIE,[e] %	57.0	35.0	40.0	12.0	50.0	63.0	55.0	65.0	14.0	1.0	0.0	1.0	5.0	48.0	25	40
Carbonate during CIE,[e] %	45.0	29.0	49.0	43.0	13.0	78.0	8.0	45.0	11.0	11.0	11.0	4.0	10.0	3.0	2	2
Organic carbon pre-CIE,[f] %	0.20	0.23	0.10	NA	0.10	NA	0.10	0.10	0.25	0.20	0.10	0.31	0.47	0.10	NA	0.2
Organic carbon during CIE,[f] %	0.20	2.62	0.35	NA	0.94	NA	0.20	0.70	0.40	0.16	0.16	0.37	0.58	0.10	NA	0.3
Carbonate ratio x sed rate ratio,[g] %	**3.3**	**5.2**	**5.3**	**17.9**	**0.1**	**3.7**	**1.2**	**2.1**	**0.1**	**42.3**	**>73**	**9.5**	**8.8**	**0.2**	**0.1**	**0.2**
TOC ratio x sed rate ratio,[h] %	**4.2**	**72.2**	**15.2**	NA	**4.7**	NA	**16.0**	**21.0**	**0.3**	**3.1**	**29.9**	**2.8**	**5.4**	**3.4**	NA	**7.8**
Reference[i]	1	2	2	3	4	5	4	4	6	7	7	8	7	9	10	9

[a]This only includes sections with a published biostratigraphic age model, a $\delta^{13}C$ record, and percent TOC and/or percent carbonate records. Sed rate stands for sedimentation rate.
[b]Background sedimentation rate (estimated based on biostratigraphy).
[c]Sedimentation rate during the CIE, estimated by dividing the thickness of the CIE by 220 ka.
[d]Ratio of sedimentation rates (CIE over background).
[e]Average percent $CaCO_3$.
[f]Average percent TOC.
[g]Estimate of $CaCO_3$ burial change during the CIE, based on the ratio of percent $CaCO_3$ times the ratio of sedimentation rates.
[h]Estimate of organic matter burial change during the CIE, based on the ratio of percent TOC times the ratio of sedimentation rates.
[i]Sources are as follows: 1, *Lu et al.* [1998]; 2, *Bolle et al.* [2000c]; 3, *Bolle et al.* [1999]; 4, *Bolle et al.* [2000a]; 5, *Bolle et al.* [2000b]; 6, *Crouch et al.* [2003]; 7, this paper; 8, *Zachos et al.* [2006]; 9, *Bolle et al.* [1998b] and *Schmitz et al.* [2001]; and 10, *Gawenda et al.* [1999] and *Schmitz et al.* [2001].
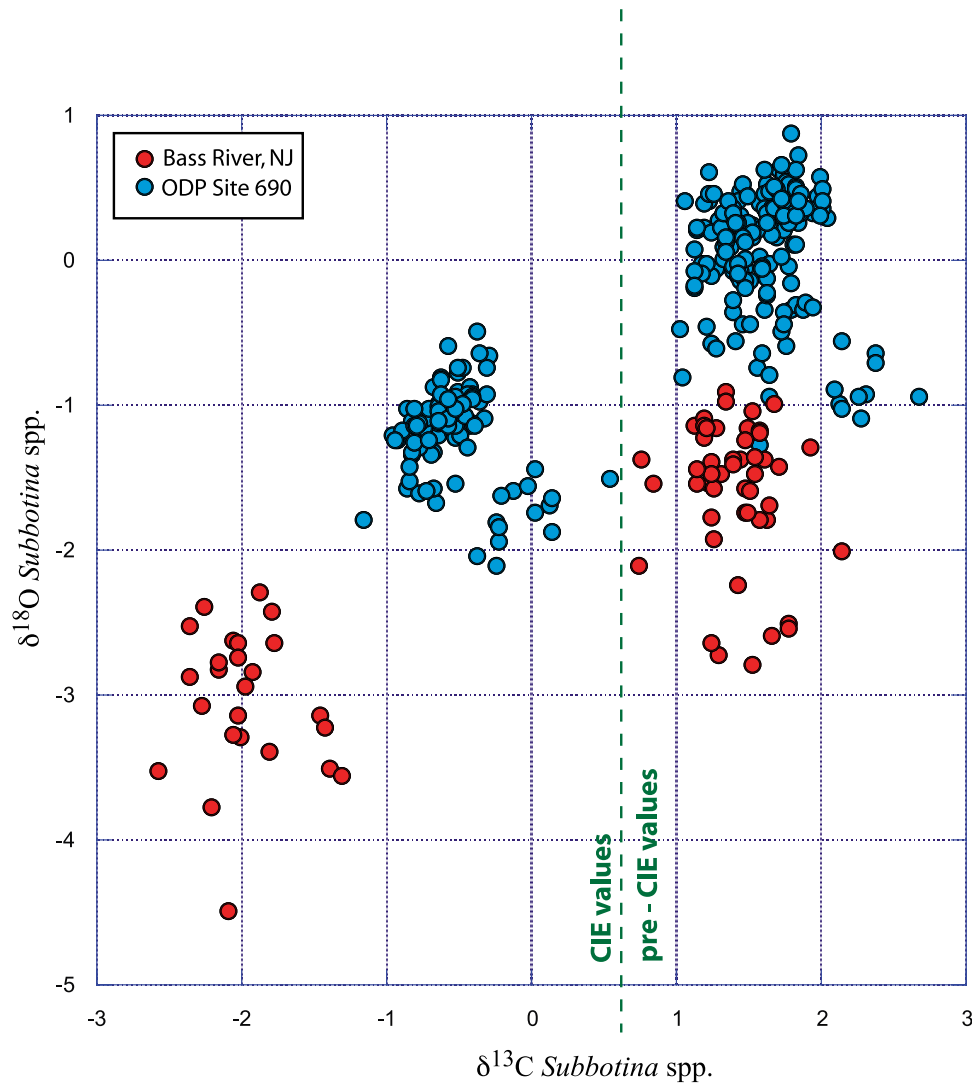
Figure 8. Crossplot of $\delta^{18}O$ versus $\delta^{13}C$ data for single-specimen analysis of *Subbotina* spp. at Bass River (this study) and open ocean ODP Site 690 [*Thomas et al.*, 2002]. Note the similarity in $\delta^{13}C$ values pre-CIE, while the average CIE values at Bass River are about 1.3‰ lighter than at Site 690.

was a regional exception. Likewise, the sections investigated here lack any clear evidence of hiatus at the onset of the CIE: scoured surfaces are not present, extensive dissolution of carbonate is not evident, and the sedimentation appears reasonably continuous. Interestingly, the "steps" in the $\delta^{13}C_{bulk\ carbonate}$ at ODP Site 690 are not represented in single-specimen isotope records [*Thomas et al.*, 2002]. We therefore suggest that the pelagic bulk carbonate carbon isotope records do not accurately reflect the rate of the CIE in the surface ocean. Either dissolution or reworking or some combination of the two tends to smear the CIE as reconstructed from bulk sediment analyses. However, these uncertainties hamper an absolute correlation of the first ~20 ka of the CIE between our records and deep-sea records.

5.2. Changes in Burial Rates and Implications for the PETM Carbon Cycle

[31] The thickness of the excursion layer in our shelf sections is a function of proximity to the coast (Figure 9); the excursion layers are thickest on the inner shelf (14 m thick at Wilson Lake [*Zachos et al.*, 2006]), intermediate on the outer shelf (11–12 m thick at Bass River and Lodo Gulch), and thinnest on the slope (5 m thick at Tumey Gulch). *Nicolo et al.* [2007] demonstrated that the trend observed on the shelf was opposite to changes in the deep sea where sedimentation rates decrease over the lower portion of the CIE [*Röhl et al.*, 2000] because of ocean acidification and carbonate dissolution, although accumulation rates eventually increase during the recovery phase [*Farley and Eltgroth*, 2003]. Our results suggest that sedimentation rates on the
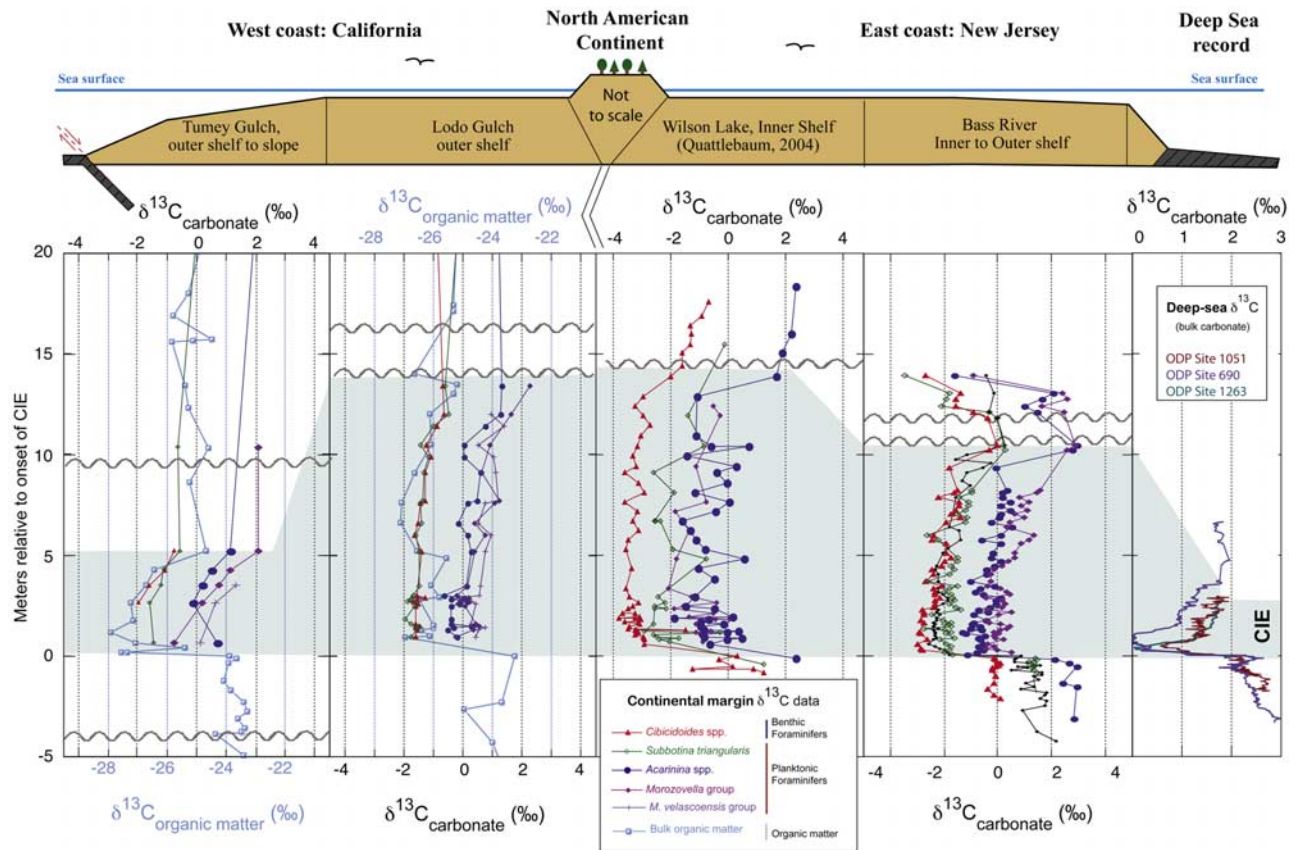
Figure 9. Summary of the carbon isotope results obtained in this and other studies and conceptual cross section from the continent to the deep sea. Data from left to right are for Tumey Gulch (continental slope, California), Lodo Gulch (outer shelf, California), Wilson Lake (inner shelf, New Jersey), Bass River (inner to outer shelf, New Jersey), and various deep-sea records (ODP Sites 1051, 690, and 1263).

continental margin increased by a factor of 5 to 11 during the PETM (Table 2).

[32] The expanded nature of the CIE is not unique to the North American margins. Sections with a thick CIE interval have been documented on the margins of the eastern Atlantic basin [*Lu et al.*, 1998], the North Sea [*Steurbaut et al.*, 2003], around the perimeter of the Tethys in Spain [*Bolle et al.*, 1998b; *Gawenda et al.*, 1999; *Schmitz et al.*, 2001], Kazakhstan and Uzbekistan [*Bolle et al.*, 2000c], Tunisia [*Bolle et al.*, 1998a], Israel [*Bolle et al.*, 2000b], Egypt [*Bolle et al.*, 2000a], in the pre-Alps [*Giusberti et al.*, 2007] and around New Zealand [*Crouch et al.*, 2003; *Nicolo et al.*, 2007]. Sections in Spain [*Schmitz et al.*, 2001], in the pre-Alps [*Giusberti et al.*, 2007] in New Zealand [*Crouch et al.*, 2003; *Nicolo et al.*, 2007], also show increases in sedimentation rates within the CIE by a factor of 2 to 5 (see Table 4 for a compilation of shelf data).

[33] Two mechanisms that could trigger increased sedimentation rates on a global scale are (1) sea level

changes and (2) increase in sediment supply. In general, sea level rose from the late Paleocene to early Eocene [*Miller et al.*, 1998a; *Speijer and Morsi*, 2002; *Sluijs et al.*, 2006; *Scheibner et al.*, 2007]. For instance, at Lodo Gulch the sediments become finer at the onset of the CIE, and a glauconitic sand layer truncates the recovery interval. At Bass River and Wilson Lake, the glauconite-rich silt to sand lithologies below the CIE have been interpreted as a transgressive systems track and the more silty lithologies above the CIE as a highstand systems track [*Miller et al.*, 1998a]. Higher sea level would provide greater accommodation space during the transgression, and progradation of the facies basinward. However, *Miller et al.* [1998a] have pointed out that sedimentation on the New Jersey margin was not only paced by changes in eustasy, but also by changes in sediment supply.

[34] We believe that the widespread rise in sedimentation rates during the CIE resulted in part from sea level rise, but also largely from an increase in the flux of fine terrigenous sediment. In climate simulations, the hydrologic cycle
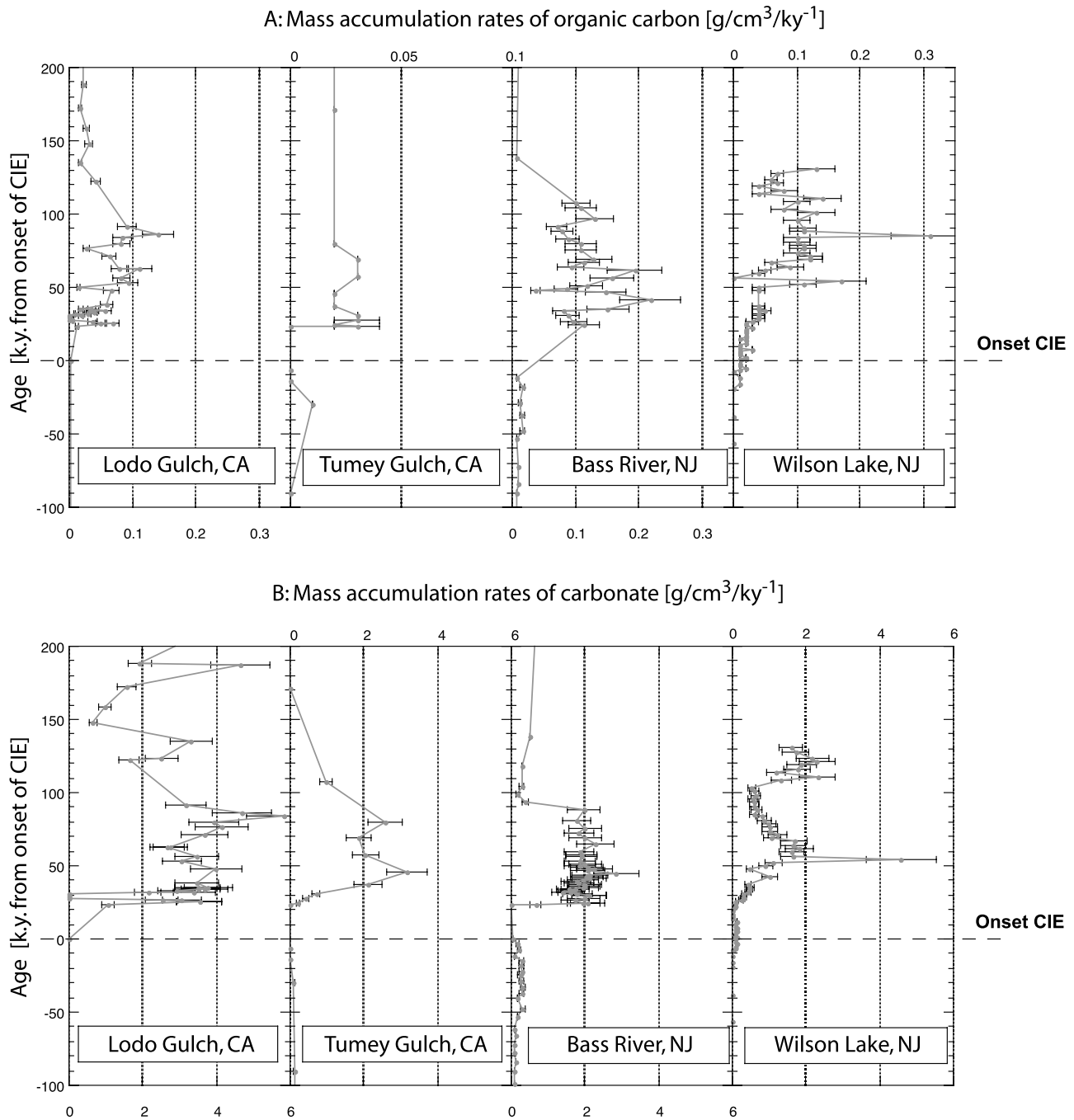
A: Mass accumulation rates of organic carbon [g/cm^3/ky^{-1}]

B: Mass accumulation rates of carbonate [g/cm^3/ky^{-1}]

Figure 10. Mass accumulation rates (MARs) of (a) organic carbon and (b) carbonate versus age (in ka from onset of the CIE). Organic carbon content used for calculating the MAR$_{organic\ matter}$ at Bass River is from *Cramer* [1999]. The error bars represent the uncertainty linked to determining bulk density based on estimated porosities (the lower estimate is for the "silt" curve, and the upper estimate is for the "clay" curve [*Bryant et al.*, 1981]). Data points represent average MAR estimates discussed here.

becomes more energetic as CO_2 and temperature rise, resulting in increased precipitation in tropical and high-latitude regions, and decreased precipitation in the subtropics [*Intergovernmental Panel on Climate Change*, 2001]. The record of the PETM is consistent with an enhanced hydrological cycle, with intensified chemical weathering and runoff [*Robert and Chamley*, 1991; *Pagani et al.*, 2006b; *Clechenko et al.*, 2007] as well as increased seasonality, which must lead to more efficient
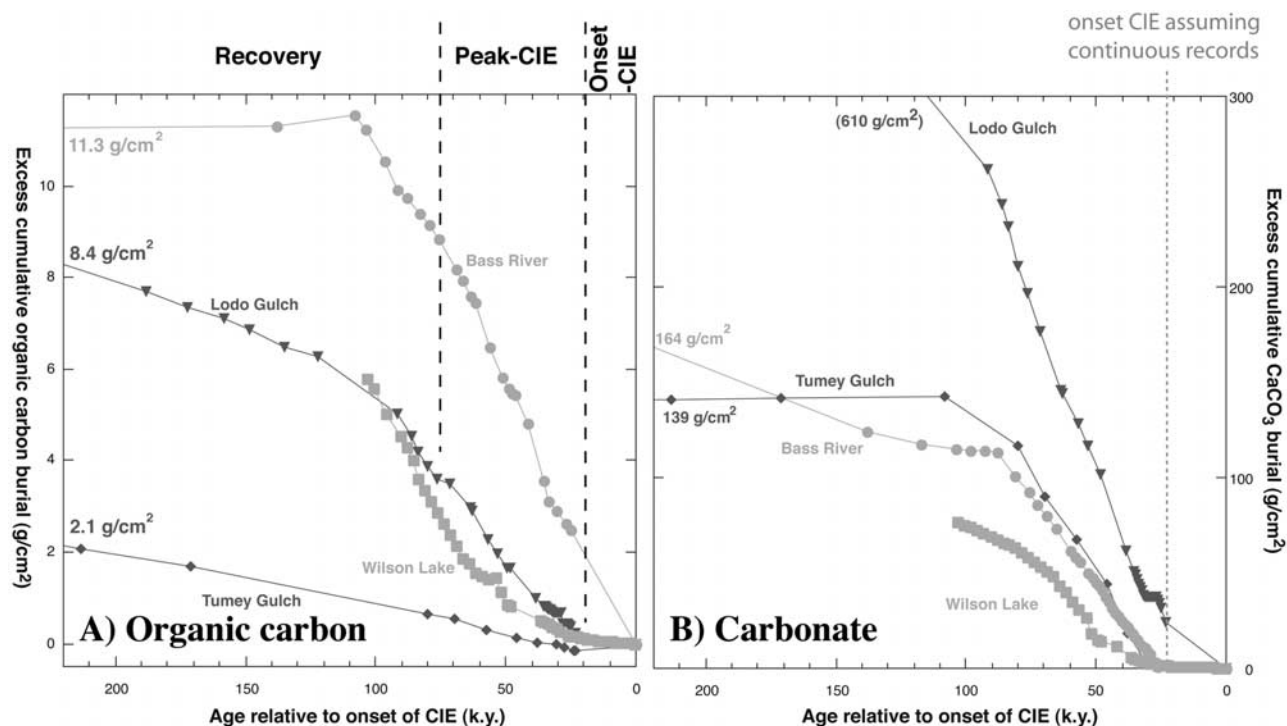
Figure 11. Excess cumulative mass accumulation rates (g cm^{-2}) of (a) organic carbon and (b) CaCO$_3$ versus age (in ka from onset of the CIE). These rates represent carbon accumulated during the CIE in excess of Paleocene accumulation. The gray dashed line in Figure 11b represents the onset of the CIE at Bass River, Lodo Gulch, and Tumey Gulch assuming sedimentation across the CIE at these locations is continuous.

physical weathering and erosion [*Schmitz and Pujalte*, 2003, 2007]. The net result would be an increase in the sediment loads of rivers and sediment supply to the continental margins, consistent with our observations.

[35] Because modern continental shelves represent the largest sink for particulate organic matter [*Ver et al.*, 1999], an important implication of increased sedimentation rates, is increased carbon burial. Many studies have highlighted the link between increased sedimentation rate, increase clay minerals in the sediment fabric, and enhanced organic matter burial and preservation, even in the absence of increased productivity [see, e.g., *Ingall and van Cappellen*, 1990; *Baldock and Skjemstad*, 2000; *Curry et al.*, 2007]. Other processes should also impact carbon burial on continental margins. Primary productivity in coastal waters in some regions increased because of higher nutrient content [*Gibbs et al.*, 2006], and evidence exist for an increase in the transport of terrigenous organic matter to the coastal ocean [*Crouch et al.*, 2003]. Furthermore, the warmer, more stratified coastal oceans might have been suboxic [*Speijer and Wagner*, 2000; *Sluijs et al.*, 2006, 2008; *Kopp et al.*, 2007; *Lippert and Zachos*, 2007], and thus more prone to preserving organic matter, thus contributing to greater carbon burial on the margin during the PETM.

[36] Indeed, mass accumulation rates rise on both shelves with both organic carbon and CaCO$_3$ burial increasing by at least an order of magnitude (Table 2 and Figure 10). Interestingly, all of the records show maximum accumula-

tion starting roughly 30 ka post-CIE and lasting until about 100 ka post-CIE. This is consistent with a slight time lag between the onset of the carbon input and the sedimentological response of the continent shelf system. Judging from previously published continental margin sections and factoring changes in sedimentation rates, we estimate that organic carbon burial during the CIE increased in nearly all shelf sections (Table 4).

[37] How much carbon could have been removed from the ocean-atmosphere system through accelerated organic carbon burial on the shelf? A plot of cumulative excess organic carbon burial suggests that the North American shelf sections stored on average between 8.1 g cm^{-12} and 11.3 g cm^{-2} more organic carbon during the PETM than they would have during a similar time interval in the Paleocene (Figure 11a). Data from the Tumey Gulch section suggest that this continental slope location may have trapped an additional 2.1 g cm^{-2} organic carbon (Figure 11a). Extrapolating these numbers to account for the total excess organic carbon burial on continental margins is not trivial, mainly because continental margins are very heterogeneous in nature and the actual flux of organic carbon will be highly dependent on local and regional factors. Even for the modern carbon cycle, quantifying carbon fluxes for the coastal ocean has proved difficult [*Borges*, 2005].

[38] We can, however, approximate to a first-order organic carbon burial on the shelves, and assess whether changes across the PETM were important to the overall

carbon budget. For this, we use a modern continental shelf area of 26×10^6 km^2 [*Walsh*, 1991], which with lower sea level is roughly 50 to 75% that of the early Eocene shelf area. Extrapolating our accumulation rate data for this surface area indicates that, for the duration of the PETM, the shelf would have accumulated between 2200 and 2900 gigatons of organic carbon (10^9 metric tons (Gt) C) in excess of pre-PETM accumulation rates. This is within the same order of magnitude as estimates of the mass of carbon released at the onset of the PETM, which range from 1500 to 2200 Gt C [*Dickens et al.*, 1997] to greater than 4500 Gt C [*Zachos et al.*, 2005]. Theoretical and empirical evidence suggest sequestration of carbon and recovery from the peak CIE interval was driven by increased continental weathering and subsequent inorganic carbon burial in the deep sea [*Dickens et al.*, 1997; *Bains et al.*, 2000; *Ravizza et al.*, 2001]. Our site compilation (Table 4) suggests an additional, albeit smaller feedback: accelerated sedimentation and increased productivity and preservation increased organic carbon burial on the shelf. Moreover, our C:N ratio values [*Crouch et al.*, 2003] support previous works suggesting that some of the organic carbon trapped on the margins originated from the terrestrial biosphere.

[39] The other important contribution to carbon fluxes is the burial of inorganic carbon as calcium carbonate. Cumulative excess CaCO$_3$ accumulation (Figure 10b) show that North American shelf sediments stored excess CaCO$_3$ during the peak CIE, a time when the deep sea was undersaturated with respect to CO$_3^{-2}$ and the CCD was shoaled to <1 km [*Zachos et al.*, 2005]. Between 60 and 110 ka, excess carbonate accumulation continued to rise on the continental margin but the slope of the curve gradually became flatter. Finally, when the deep sea returned to pre-event carbonate ion levels (>110 ka) the excess accumulation of carbonate at Tumey Gulch, Bass River and Wilson Lake stabilized. At Lodo Gulch, excess carbonate accumulation continued to increase throughout the Eocene, indicating regional heterogeneities in carbonate production and preservation after the end of the CIE. Nevertheless, the consistent pattern emerging is that carbonate burial on the shelf also increased significantly during the CIE, and then subsided at most locations during the later phase of the CIE at a time when carbonate deposition shifted to the deep ocean. This is supported by the compilation of data (Table 4) showing an overall increase in carbonate flux in the majority of the shallower sections of the continental shelf. At many sites (Table 4), carbonate content in the rock decreases even as carbonate accumulation increases because of the elevated sedimentation rates. The reduction in carbonate content mostly reflects dilution by siliciclastics rather than dissolution (as in the deep sea). The long-term effect of carbonate burial is to trap CO$_3^{-2}$ derived from continental weathering [*Ridgwell and Zeebe*, 2005]. Thus, the shelf acted as a net sink for atmospheric carbon over the duration of the CIE, both in the form of calcium carbonate and particulate organic matter.

[40] The increase in carbonate burial on the shelf might have been driven by higher CO$_3^{-2}$ saturation resulting from increased continental runoff during the recovery interval as observed in the deep sea [*Zachos et al.*, 2005]. However, the coastal ocean is typically oversaturated with respect to CO$_3^{-2}$, and so this mechanism is unlikely to significantly alter rates of mineralization on the shelf. We suspect instead that the increase in carbonate burial is largely linked to the background increase in siliciclastic clay flux; this would have accelerated burial of carbonate and retarded dissolution, thus accounting for the excess carbonate. Regardless of cause, the increased organic carbon and carbonate burial rates on the shelf need to be considered in computations of the global balance of carbon fluxes across the Paleocene-Eocene boundary. Inclusion of the shelf fluxes may, for example, help resolve the discrepancy of the mass of carbon released as estimated from isotopes and carbonate accumulation records [see *Pagani et al.*, 2006a].

6. Summary

[41] We document a ~3.0–4.5‰ CIE on North American shelves, which is similar to pelagic planktonic records, larger than most pelagic bulk carbonate records, but still less than continental records. This supports the hypothesis that deep-sea bulk carbonate records are often truncated by dissolution and/or reworking, and that the continental soil nodule and organic carbon δ^{13}C signal is amplified by increased fractionation. Because productivity and sedimentation rates increased dramatically across the CIE, the midlatitude continental shelves sequestered carbonate and organic carbon more efficiently during the CIE than during the upper Paleocene. Excess organic carbon burial on the midlatitude shelves may have sequestered a significant portion of the released CO$_2$, and thus may have contributed significantly to the CIE recovery. The role of inorganic carbon burial on the carbon budget is more difficult to assess and would depend on the phasing between carbonate dissolution in the deep sea and carbonate accumulation on the shelf, though it is possible that increased carbonate burial on the shelf partially countered the effects of carbonate dissolution in the deep sea. Because increased sedimentation rates were probably linked to increased continental weathering and erosion of land deposits, a more active hydrological cycle served as important negative feedback on the CIE and associated warming by promoting carbon burial.

References

Bains, S., R. D. Norris, R. M. Corfield, and K. L. Faul (2000), Termination of global warmth at the Paleocene/Eocene boundary through productivity feedback, *Nature*, *407*, 171–174, doi:10.1038/35025035.

Baldock, J. A., and J. O. Skjemstad (2000), Role of the soil matrix and minerals in protecting natural organic materials against biological attack, *Org. Geochem.*, *31*, 697–710, doi:10.1016/S0146-6380(00)00049-8.

Bartow, A. J. (1991), *The Cenozoic Evolution of the San Joaquin Valley, California*, Gov. Print. Off., Washington, D. C.

Bemis, B. E., H. J. Spero, J. Bijma, and D. W. Lea (1998), Reevaluation of the oxygen isotopic composition of planktonic foraminifera: Experimental results and revised paleotemperature equations, *Paleoceanography*, *13*, 150–160, doi:10.1029/98PA00070.

Berggren, W. A., and J. Aubert (1983), Paleocene benthic foraminiferal biostratigraphy and paleobathymetry of the central Coast Ranges of California, in *Studies in Tertiary Stratigraphy of the California Coast Ranges*, edited by E. E. Brabb, *U.S. Geol. Surv. Pap.*, *1213*, 4–21.

Berggren, W. A., D. V. Kent, M. P. Aubry, and J. Hardenbol (1995), Geochronology, time scales and global stratigraphic correlation: Unified temporal framework for an historical geology, in *Geochronology, Time Scales and Global Stratigraphic Correlation*, edited by W. A. Berggren et al., pp. v–vi, Soc. for Sediment. Geol., Tulsa, Okla.

Bolle, M.-P., T. Adatte, G. Keller, K. Von Salis, and S. J. Burns (1998a), The Paleocene-Eocene transition in the southern Tethys (Tunisia): Climatic and environmental fluctuations, *Bull. Soc. Geol. Fr.*, *170*, 661–680.

Bolle, M.-P., T. Adatte, G. Keller, K. Von Salis, and J. Hunziker (1998b), Biostratigraphy, mineralogy and geochemistry of the Trabakua Pass and Ermua sections in Spain: Paleocene-Eocene transition, *Eclogae Geol. Helv.*, *91*, 1–25.

Bolle, M.-P., A. A. Tantawy, A. Pardo, T. Adatte, S. J. Burns, and A. Kassab (2000a), Climatic and environmental changes documented in the upper Paleocene to lower Eocene of Egypt, *Eclogae Geol. Helv.*, *93*, 33–51.

Bolle, M.-P., A. Pardo, T. Adatte, K. Von Salis, and S. Burns (2000b), Climatic evolution on the southeastern margin of the Tethys (Negev, Israel) from the Palaeocene to the early Eocene: Focus on the late Paleocene thermal maximum, *J. Geol. Soc. London*, *157*, 929–941.

Bolle, M.-P., A. Pardo, K.-U. Hinrichs, T. Adatte, K. Von Salis, S. Burns, and N. Muzylev (2000c), The Paleocene-Eocene transition in the marginal northeastern Tethys (Kazakhstan and Uzbekistan), *Int. J. Earth Sci.*, *89*, 390–414, doi:10.1007/s005310000092.

Borges, A. V. (2005), Do we have enough pieces of the jigsaw to integrate CO_2 fluxes in the coastal ocean?, *Estuaries*, *28*, 3–27.

Bowen, G. J., D. J. Beerling, P. L. Koch, J. C. Zachos, and T. Quattlebaum (2004), A humid climate state during the Palaeocene/Eocene thermal maximum, *Nature*, *432*, 495–499, doi:10.1038/nature03115.

Bryant, W. R., R. Bennett, and C. Katherman (1981), Shear strength, consolidation, porosity, and permeability of oceanic sediments, in *The Sea*, vol. 7, edited by C. Emiliani, pp. 1555–1616, John Wiley, New York.

Bujak, J. P., and H. Brinkhuis (1998), Global warming and dinocyst changes across the Paleocene/Eocene epoch boundary, in *Late Paleocene–Early Eocene Climatic and Biotic Events in the Marine and Terrestrial Records*, edited by M.-P. Aubry et al., pp. 277–295, Columbia Univ. Press, New York.

Clechenko, E. R., D. C. Kelly, G. J. Harrington, and C. A. Stiles (2007), Terrestrial records of a regional weathering profile at the Paleocene-Eocene boundary in the Williston Basin of North Dakota, *Geol. Soc. Am. Bull.*, *119*, 428–442, doi:10.1130/B26010.1.

Cramer, B. S. (1999), The late Paleocene thermal maximum, Bass River, NJ: Neritic response to a runaway greenhouse event, M. S. thesis, 132 pp., Rutgers State Univ. of N. J., New Brunswick.

Cramer, B. S., M.-P. Aubry, K. G. Miller, R. K. Olsson, J. D. Wright, and D. V. Kent (1999), An exceptional chronologic, isotopic, and clay mineralogic record of the latest Paleocene thermal maximum, Bass River, NJ, ODP 174AX, *Bull. Soc. Geol. Fr.*, *170*, 883–897.

Crouch, E., C. Heilmann, H. Brinkhuis, H. Morgans, K. Rogers, H. Egger, and B. Schmitz (2001), Global dinoflagellate event associated with the late Paleocene thermal maximum, *Geology*, *29*, 315–318, doi:10.1130/0091-7613(2001)029<0315:GDEAWT>2.0.CO;2.

Crouch, E., G. R. Dickens, H. Brinkhuis, M.-P. Aubry, C. J. Hollis, K. M. Rogers, and H. Visscher (2003), The *Apectodinium* acme and terrestrial discharge during the Paleocene-Eocene thermal maximum: New palynological, geochemical and calcareous nannoplankton observations at Tawanui, New Zealand, *Palaeogeogr. Palaeoclimatol. Palaeoecol.*, *194*, 387–403, doi:10.1016/S0031-0182(03)00334-1.

Curry, K. J., R. Bennett, L. M. Mayer, A. Curry, M. Abril, P. M. Biesiot, and M. H. Hulbert (2007), Direct visualization of clay microfabric signatures driving organic matter preservation in fine-grained sediment, *Geochim. Cosmochim. Acta*, *71*, 1709–1720, doi:10.1016/j.gca.2007.01.009.

D'Hondt, S., J. C. Zachos, and G. Schultz (1994), Stable isotopic signals and photosymbiosis in late Paleocene planktic foraminifera, *Paleobiology*, *20*(3), 391–406.

Dickens, G. R., J. R. O'Neil, D. K. Rea, and R. M. Owen (1995), Dissociation of oceanic methane hydrate as a cause of the carbon isotope excursion at the end of the Paleocene, *Paleoceanography*, *10*, 965–971.

Dickens, G. R., M. M. Castillo, and J. C. G. Walker (1997), A blast of gas in the latest Paleocene: Simulating first-order effects of massive dissociation of oceanic methane hydrate, *Geology*, *25*, 259–262, doi:10.1130/0091-7613(1997)025<0259:ABOGIT>2.3.CO;2.

Engebretson, D. C., A. Cox, and R. G. Gordon (1985), Relative motions between oceanic and continental plates in the Pacific Basin, *Spec. Pap. Geol. Soc. Am.*, *206*, 59 pp.

Farley, K. A., and S. F. Eltgroth (2003), An alternative age model for the Paleocene-Eocene thermal maximum using extraterrestrial [3]He, *Earth Planet. Sci. Lett.*, *208*, 135–148, doi:10.1016/S0012-821X(03)00017-7.

Gawenda, P., W. Winkler, B. Schmitz, and T. Adatte (1999), Climate and bioproductivity control on carbonate turbidite sedimentation (Paleocene to earliest Eocene, Gulf of Biscay, Zumaia, Spain), *J. Sediment. Res.*, *69*, 1253–1261.

Gibbs, S., T. J. Bralower, P. R. Brown, J. C. Zachos, and L. Bybell (2006), Shelf and open-ocean calcareous phytoplankton assemblages across the Paleocene-Eocene thermal maximum: Implications for global productivity gradients, *Geology*, *34*, 233–236, doi:10.1130/G22381.1.

Gibson, T. G., L. M. Bybell, and D. B. Mason (2000), Stratigraphic and climatic implications of clay mineral changes around the Paleocene/Eocene boundary of the northeastern US margin, *Sediment. Geol.*, *134*, 65–92, doi:10.1016/S0037-0738(00)00014-2.

Giusberti, L., D. Rio, C. Agnini, J. Backman, E. Fornaciari, F. Tateo, and M. Oddone (2007), Mode and tempo of the Paleocene-Eocene thermal maximum in an expanded section from the Venetian pre-Alps, *Geol. Soc. Am. Bull.*, *119*, 391–412, doi:10.1130/B25994.1.

Harris, D., W. R. Horwáth, and C. van Kessel (2001), Acid fumigation of soils to remove carbonates prior to total organic carbon or carbon-13 isotopic analysis, *Soil Sci. Soc. Am. J.*, *65*, 1853–1856.

Ingall, E. D., and P. van Cappellen (1990), Relation between sedimentation rate and burial of organic phosphorus and organic carbon in marine sediments, *Geochim. Cosmochim. Acta*, *54*, 373–386, doi:10.1016/0016-7037(90)90326-G.

Intergovernmental Panel on Climate Change (2001), *Climate Change 2001: The Scientific Basis*, edited by J. T. Houghton et al., 881 pp., Cambridge Univ. Press, Cambridge, U. K.

Kelly, D. C., T. J. Bralower, and J. C. Zachos (2001), On the demise of the early Paleogene *Morozovella velascoensis* lineage: Terminal progenesis in the planktonic Foraminifera, *Palaios*, *16*, 507–523.

Kelly, D. C., J. C. Zachos, T. J. Bralower, and S. A. Schellenberg (2005), Enhanced terrestrial weathering/runoff and surface ocean carbonate production during the recovery stages of the Paleocene-Eocene thermal maximum, *Paleoceanography*, *20*, PA4023, doi:10.1029/2005PA001163.

Kennett, J. P., and L. D. Stott (1991), Abrupt deep-sea warming, paleoceanographic changes and benthic extinctions at the end of the Paleocene, *Nature*, *353*, 225–229, doi:10.1038/353225a0.

Koch, P. L., J. C. Zachos, and P. D. Gingerich (1992), Correlation between isotope records in marine and continental carbon reservoirs near the Paleocene/Eocene boundary, *Nature*, *358*, 319–322, doi:10.1038/358319a0.

Kopp, R. E., T. D. Raub, D. Schumann, V. Hojatollah, A. V. Smirnov, and J. L. Kirschvink (2007), Magnetofossil spike during the Paleocene-Eocene thermal maximum: Ferromagnetic resonance, rock magnetic, and electron microscopy evidence from Ancora, New Jersey, United States, *Paleoceanography*, *22*, PA4103, doi:10.1029/2007PA001473.

Kraus, M. J., and S. Riggins (2007), Transient drying during the Paleocene-Eocene thermal maximum (PETM): Analysis of paleosols in the bighorn basin, Wyoming, *Palaeogeogr. Palaeoclimatol. Palaeoecol.*, *245*, 444–461, doi:10.1016/j.palaeo.2006.09.011.

Lippert, P. C., and J. C. Zachos (2007), A biogenic origin for anomalous fine-grained magnetic material at the Paleocene-Eocene boundary at Wilson Lake, New Jersey, *Paleoceanography*, *22*, PA4104, doi:10.1029/2007PA001471.

Lu, G., T. Adatte, G. Keller, and N. Ortiz (1998), Abrupt climatic, oceanographic and ecological changes near the Paleocene-Eocene transition in the deep Tethys basin: The Alademilla section, southern Spain, *Eclogae Geo. Helv.*, *91*, 293–306.

Martin, L. T. (1943), Eocene foraminifera from the type Lodo Formation Fresno County, California, *Stanford Univ. Publ. Geol. Sci.*, *3*, 93–125.

Martini, E. (1971), Standard Tertiary and Quaternary calcareous nannoplankton zonation, in *Proceedings of the II Planktonic Conference*, vol. 2, edited by A. Farinacci, pp. 739–785, Tecnoscienza, Rome.

Miller, K. G., G. S. Mountain, J. V. Browning, M. Kominz, P. J. Sugarman, N. Christie-Blick, M. E. Katz, and J. D. Wright (1998a), Cenozoic global sea level, sequences, and the New Jersey transect: Results from coastal plain and continental slope drilling, *Rev. Geophys.*, *36*, 569–601, doi:10.1029/98RG01624.

Miller, K. G., et al. (1998b), *Proceedings of the Ocean Drilling Program, Initial Reports, Leg 174AX*, Ocean Drill. Program, College Station, Tex.

Miller, K. G., P. J. Sugarman, J. V. Browning, M. A. Kominz, R. K. Olsson, M. D. Feigenson, and J. C. Hernandez (2004), Upper Cretaceous sequences and sea-level history, New Jersey coastal plain, *Geol. Soc. Am. Bull.*, *116*, 368–393, doi:10.1130/B25279.1.

Mountain, G. S., et al. (Eds.) (1994), *Initial Reports, New Jersey Continental Slope and RiseSites 902–906*, vol. 150, Ocean Drill. Program, College Station, Tex.

Nicolo, M., G. R. Dickens, C. J. Hollis, and J. C. Zachos (2007), Multiple early Eocene hyperthermals: Their sedimentary expression on the New Zealand continental margin and in the deep sea, *Geology*, *35*, 699–702, doi:10.1130/G23648A.1.

Pagani, M., K. Caldeira, D. Archer, and J. C. Zachos (2006a), An ancient carbon mystery, *Nature*, *314*, 1556–1557.

Pagani, M., et al. (2006b), Arctic hydrology during global warming at the Palaeocene/Eocene thermal maximum, *Nature*, *442*, 671–675, doi:10.1038/nature05043.

Paillard, D., L. Labeyrie, and P. Yiou (1996), Macintosh program performs time-series analysis, *Eos Trans. AGU*, *77*, 379, doi:10.1029/96EO00259.

Perch-Nielsen, K. (1985), Mesozoic calcareous nannofossils, in *Plankton Stratigraphy*, edited by H. M. Bolli, pp. 329–426, Cambridge Univ. Press, New York.

Quattlebaum, T. G. (2004), The environmental impact of the Paleocene-Eocene thermal maximum on the coastal ocean: A multi-proxy approach, Master's thesis, 98 pp., Univ. of Calif., Santa Cruz.

Ravizza, G., R. D. Norris, J. Blutsztajn, and M.-P. Aubry (2001), An osmium isotope excursion associated with the late Paleocene thermal maximum: Evidence of intensified chemical weathering, *Paleoceanography*, *16*, 155–163, doi:10.102/2000PA000541.

Ridgwell, A., and R. E. Zeebe (2005), The role of the global carbonate cycle in the regulation and evolution of the Earth system, *Earth Planet. Sci. Lett.*, *234*, 299–315, doi:10.1016/j.epsl.2005.03.006.

Robert, C., and H. Chamley (1991), Development of early Eocene warm climates, as inferred from clay mineral variation in oceanic sediments, *Global Planet. Change*, *3*, 315–332, doi:10.1016/0921-8181(91)90114-C.

Robert, C., and J. P. Kennett (1994), Antarctic subtropical humid episode at the Paleocene-Eocene boundary: Clay mineral evidence, *Geology*, *22*, 211–214.

Röhl, U., T. J. Bralower, R. D. Norris, and G. Wefer (2000), New chronology for the late Paleocene thermal maximum and its environmental implications, *Geology*, *28*, 927–930, doi:10.1130/0091-7613(2000)28<927: NCFTLP>2.0.CO;2.

Scheibner, C., M. W. Rasser, and M. Mutti (2007), The Campo section (Pyrenees, Spain) revisited: Implications for changing benthic carbonate assemblages across the Paleocene-Eocene boundary, *Palaeogeogr. Palaeoclimatol. Palaeoecol.*, *248*, 145–168, doi:10.1016/j.palaeo.2006.12.007.

Schmitz, B., and V. Pujalte (2003), Sea-level, humidity, and land-erosion records across the initial Eocene thermal maximum from a continental-marine transect in northern Spain, *Geology*, *31*, 689–692, doi:10.1130/G19527.1.

Schmitz, B., and V. Pujalte (2007), Abrupt increase in seasonal extreme precipitation at the Paleocene-Eocene boundary, *Geology*, *35*, 215–218, doi:10.1130/G23261A.1.

Schmitz, B., V. Pujalte, and K. Núñez-Betelu (2001), Climate and sea-level perturbations during the incipient Eocene thermal maximum: Evidence from siliciclastic units in the Basque Basin (Ermua, Zumaia and Trabakua Pass), northern Spain, *Palaeogeogr. Palaeoclimatol. Palaeoecol.*, *165*, 299–320, doi:10.1016/S0031-0182(00)00167-X.

Schouten, S., E. C. Hopmans, E. Schefuss, and J. S. S. Damste (2002), Distributional variations in marine crenarchaeotal membrane lipids: A new tool for reconstructing ancient sea water temperatures?, *Earth Planet. Sci. Lett.*, *204*, 265–274, doi:10.1016/S0012-821X(02)00979-2.

Schouten, S., M. Woltering, W. I. C. Rijpstra, A. Sluijs, H. Brinkhuis, and J. S. Sinninghe Damsté (2007), The Paleocene-Eocene carbon isotope excursion in higher plant organic matter: Differential stable carbon isotopic fractionation of angiosperms and conifers on the Arctic continent, *Earth Planet. Sci. Lett.*, *258*, 581–592, doi:10.1016/j.epsl.2007.04.024.

Shackleton, N. (1974), Attainment of isotopic equilibrium between ocean water temperature and the benthonic foraminifera genus *Uvigerina*; isotopic changes in the ocean during the last glacial, in *Les méthodes quantitatives d'étude de variation climatique au cours du Pléistocène*, pp. 203–209, Cent. Natl. de la Rech. Sci., Paris.

Sluijs, A., et al. (2006), Subtropical Arctic Ocean temperatures during the Palaeocene/Eocene thermal maximum, *Nature*, *441*, 610–613, doi :10.1038/nature04668.

Sluijs, A., H. Brinkhuis, S. Schouten, S. Bohaty, C. M. John, J. C. Zachos, G.-J. Reichart, J. Sinninghe Damsté, E. Crouch, and G. R. Dickens (2007), Environmental change before the rapid carbon injection at the Palaeocene/Eocene boundary, *Nature*, *450*, 1218–1221, doi:10.1038/nature06400.

Sluijs, A., U. Röhl, S. Schouten, H.-J. Brumsack, F. Sangiorgi, J. S. Sinninghe Damsté, and H. Brinkhuis (2008), Arctic late Paleocene–early Eocene paleoenvironments with special emphasis on the Paleocene-Eocene thermal maximum (Lomonosov Ridge, Integrated Ocean Drilling Program Expedition 302), *Paleoceanography*, *23*, PA1S11, doi:10.1029/2007PA001495.

Speijer, R. P., and A. M. Morsi (2002), Ostracode turnover and sea-level changes associated with the Paleocene-Eocene thermal maximum, *Geology*, *30*, 23–26, doi:10.1130/0091-7613(2002)030<0023:OTASLC>2.0.CO;2.

Speijer, R. P., and T. Wagner (2000), Bursts of methane from the deep sea and the spread of anoxia into epicontinental basins at the end of the Paleocene; a causal relationship involving sea-level change, paper presented at Catastrophic Events and Mass Extinctions: Impacts and Beyond, Lunar and Planet. Inst., Vienna, 9–12 July.

Steurbaut, E., R. Magioncalda, C. Dupuis, S. Van Simaeys, E. Roche, and M. Roche (2003), Palynology, paleoenvironments, and organic carbon isotope evolution in lagoonal Paleocene-Eocene boundary settings in North Belgium, in *Causes and Consequences of Globally Warm Climates in the Early Paleogene*, edited by S. L. Wing et al., *Spec. Pap. Geol. Soc. Am.*, *369*, 291–317.

Svensen, H., S. Planke, A. Malthe-Sørenssen, B. Jamtveit, R. Myklebust, T. R. Eidem, and S. S. Rey (2004), Release of methane from a volcanic basin as a mechanism for initial Eocene global warming, *Nature*, *429*, 542–545, doi:10.1038/nature02566.

Thomas, E., and N. Shackleton (1996), The Palaeocene-Eocene benthic foraminiferal extinction and stable isotopes anomalies, in *Correlation of the Early Paleogene in Northwest Europe*, edited by R. W. O. B. Knox, R. M. Cornfield, and R. E. Dunay, pp. 401–441, Geol. Soc. of London, London.

Thomas, D. J., T. J. Bralower, and J. C. Zachos (1999), New evidence for subtropical warming during the late Paleocene thermal maximum: Stable isotopes from Deep Sea Drilling Project Site 527, Walvis Ridge, *Paleoceanography*, *14*, 561–570, doi:10.1029/1999PA900031.

Thomas, D. J., J. C. Zachos, T. J. Bralower, E. Thomas, and S. Bohaty (2002), Warming the fuel for the fire: Evidence for the thermal dissociation of methane hydrate during the Paleocene-Eocene thermal maximum, *Geology*, *30*, 1067–1070, doi:10.1130/0091-7613(2002)030<1067:WTFFTF>2.0.CO;2.

Tripati, A., and H. Elderfield (2005), Deep-sea temperature and circulation changes at the Paleocene-Eocene thermal maximum, *Science*, *308*, 1894–1898, doi:10.1126/science.1109202.

Ver, L. M., F. T. MacKenzie, and A. Lerman (1999), Biogeochemical responses of the carbon cycle to natural and human perturbations: Past, present, and future, in *Biogeochemical Cycles and Their Evolution Over Geologic Time: A Tribute to the Career of Robert A. Berner*, edited by D. E. Canfield and B. P. Bourdeau, pp. 762–801, Kline Geol. Lab., Yale Univ., New Haven, Conn.

Walsh, J. J. (1991), Importance of continental margins in the marine biogeochemical cycling of carbon and nitrogen, *Nature*, *350*, 53–55, doi:10.1038/350053a0.

White, R. T. (1938), Eocene Lodo Formation and Cerros member of California, paper presented at Meeting of the Geological Society of America, Geol. Soc. of Am., New York.

Wing, S. L., G. J. Harrington, F. A. Smith, J. I. Bloch, D. M. Boyer, and K. H. Freeman (2005), Transient floral change and rapid global warming at the Paleocene-Eocene boundary, *Science*, *310*, 993–996, doi:10.1126/science.1116913.

Zachos, J., M. Pagani, L. Sloan, E. Thomas, and K. Billups (2001), Trends, rhythms, and aberra-

tions in global climate 65 Ma to present, *Science*, *292*, 686–693, doi:10.1126/science.1059412.

Zachos, J. C., M. W. Wara, S. M. Bohaty, M. L. Delaney, M. Rose-Petrizzo, A. Brill, T. J. Bralower, and I. Premoli-Silva (2003), A transient rise in tropical sea surface temperature during the Paleocene-Eocene thermal maximum, *Science*, *302*, 1551–1554, doi:10.1126/science.1090110.

Zachos, J. C., et al. (2005), Rapid acidification of the ocean during the Paleocene-Eocene thermal maximum, *Science*, *308*, 1611–1615, doi:10.1126/science.1109004.

Zachos, J. C., S. Schouten, S. Bohaty, T. Quattlebaum, A. Sluijs, H. Brinkhuis, S. J. Gibbs, and T. J. Bralower (2006), Extreme warming of mid-latitude coastal ocean during the Paleocene-Eocene thermal maximum: Inferences from TEX$_{86}$ and isotope data, *Geology*, *34*, 737–740, doi:10.1130/G22522.1.

Zachos, J. C., S. M. Bohaty, C. M. John, H. McCarren, D. C. Kelly, and T. Nielsen (2007), The Paleocene-Eocene carbon isotope excursion: Constraints from individual shell planktonic foraminifer records, *R. Soc. Philos. Trans., Ser. A*, *365*, 1829–1842.

———————————————

S. M. Bohaty and S. Gibbs, School of Ocean and Earth Sciences, National Oceanography Centre, European Way, Southampton, SO14 3ZH, UK.

T. J. Bralower, Department of Geosciences, Deike Building, Pennsylvania State University, University Park, PA 16802, USA.

H. Brinkhuis and A. Sluijs, Palaeoecology, Institute of Environmental Biology, Utrecht University, Laboratory of Palaeobotany and Palynology, Budapestlaan 4, NL-3584 CD Utrecht, Netherlands.

C. M. John, Department of Earth Science and Engineering, Imperial College London, Exhibition Road, London, SW7 2AZ, UK. (cedric.john@imperial.ac.uk)

J. C. Zachos, Department of Earth and Planetary Sciences, University of California, Earth and Marine Sciences Building, Santa Cruz, CA 95060, USA.